FUNDAMENTAL RESEARCH REGARDING THE ULTRASONIC STIRRING EFFECTS ON THE MICROSTRUCTURE OF A356 CASTINGS

by

SHIAN JIA

LAURENTIU NASTAC, COMMITTEE CHAIR
NAGY EL-KADDAH
J. BRIAN JORDAN
MARK L. WEAVER

A THESIS

Submitted in partial fulfillment of the requirements for
the degree of Master of Science in the Department of
Metallurgical and Materials Engineering
in the Graduate School of
The University of Alabama

TUSCALOOSA, ALABAMA

2013

ABSTRACT

Ultrasonic stirring treatment (UST) of molten metal has significant effects on the solidification microstructure of A356 alloy, which includes grain structure, distribution of inclusions, refinement of secondary phases, etc. The primary causes are due to ultrasonic cavitation, acoustic streaming and propagation of ultrasound waves in media. However, the mechanism of how those effects happen are not fully understood and quantified.

In this research, molten A356 alloy was treated with high power ultrasound at a frequency of 18 kHz, and then at relatively high superheat, the melt was cast into a permanent metal mold which complies with ASTM B108-02. The UST processing system was custom built to perform the present UST study.

The relatively high superheat condition is similar to the one used in the standard foundry practice, which will assist in the scale up of practical application of ultrasonic stirring technology. The selected parameters for the ultrasonic stirring technology (UST) were determined by using an UST modeling software tool that was recently developed and validated. The UST modeling software tool is capable of modeling and simulating the acoustic streaming and ultrasonic cavitation as well as the microstructure evolution during the solidification of cast alloys.

Since the UST was preceded in the molten alloy, no dendrites are growing during the UST processing. Besides, more energy is required for homogeneous nucleation to occur. Consequently, the dominant mechanism of nucleation in this research is heterogeneous nucleation.

The microstructure and mechanical properties of the A356 alloy processed with and without UST were analyzed and compared in detail in this study. It was demonstrated that the ultrasonically-stirred A356 alloy shows superior microstructure characteristics with very low micro-porosity levels and improved tensile properties when compared with the standard A356 alloy.

LIST OF ABBREVIATIONS AND SYMBOLS

a	Cronbach's index of internal consistency
df	Degrees of freedom: number of values free to vary after certain restrictions have been placed on the data
F	Fisher's *F* ratio: A ration of two variances
M	Mean: the sum of a set of measurements divided by the number of measurements in the set
p	Probability associated with the occurrence under the null hypothesis of a value as extreme as or more extreme than the observed value
r	Pearson product-moment correlation
t	Computed value of t test
<	Less than
=	Equal to

ACKNOWLEDGMENTS

I am pleased to have this opportunity to thank the many colleagues, friends, and faculty members who have helped me with this research project. I am most indebted to Dr. Laurentiu Nastac, the chairman of this dissertation, for sharing his research expertise and wisdom regarding motivational theory. I would also like to thank all of my committee members, Dr. Mark L. Weaver, Dr. Nagy El-Kaddah, and Dr. J. Brian Jordon for their support of both the dissertation and my academic progress. I would like to thank Bob Fanning for his guidance in lab operation safety and assistance in samples obtaining. I also want to thank Xiaoda Liu and Akash Patel for their assistance in collecting data.

This research would not have been possible without the support of my friends and fellow graduate students and of course of my family who never stopped encouraging me to persist.

CONTENTS

LIST OF TABLES

LIST OF FIGURES

1.0 INTRODUCTION

Grain refinement is important for improving mechanical properties such as increasing the toughness and fracture resistance of an alloy [11; 49; 67]. Chemical refiners are usually used as the main sources for refining the structures. However, these refiners cannot be applied for every alloy and some of them forming compounds that have detrimental effects on the mechanical properties [11]. They cause melt contamination and just part of them act as nucleation sites while the rest of them turn into impurities [32]. In comparison, under some conditions, physical refinement is recommended for refining the microstructures of alloys. Physical refinement has been tried previously such as using electro-magnetic [30; 45] or magnetohydrodynamics (MHD) [66] stirring at above liquidus, shearing above liquidus temperature and ultrasonic stirring treatment (UST) [34]. Ultrasonic stirring treatment can be effectively used in commercial casting processes, e.g. direct-chill, shape or die casting due to its effects on microstructure of metals, which includes control of grain structure, variation in the distribution and refinement of secondary phases, improvement of material homogeneity, and the uniform distribution of inclusions. The existence of these effects is proven experimentally, and some of them are used in industry [5; 6]. In addition, the UST offers other advantages such as [38]:

(i) Degassing effect of melt

(ii) Integration into shape and continuous casting systems without changing basic technological parameters

(iii) Treatment time is considerably short

The earliest research of ultrasonic stirring effect on metal can date back to 1878, when Chernov [16] was trying to improve the quality of cast metal by elastic oscillations. Since then, a large amount of relevant research has been made in this field. It has been proved experimentally that UST treatment into melt metal can eliminate columnar dendritic structure, may obtain globular non-dendritic structures, and more refined microstructure [3; 4; 22; 24; 39]. Cast components with globular grains have many advantages including the decrease of hot tearing susceptibility, isotropy microstructure and properties, reduced micro-segregation due to reduced grain size, improved resistance to corrosion, and improvement of mechanical properties, such as hardness, yield strength, and elongation [23].

The mechanism of heterogeneous nucleation above liquidus is not very well understood. Three major mechanisms were proposed:

(1) Oxide nucleation, where oxides nucleate intermetallics and aluminum nucleates on them as substrate. However, this multistep nucleation [70; 25] looks vague due to high wetting contact angle of oxides with melt which is usually above 120 **°C** and occurring cohesion, not adhesion .

(2) The other method that was introduced by Eskin [17] is by nucleating aluminides, which act as nucleating sites for aluminum (e.g. Al3Ti).

(3) The other major mechanism is the occurrence of cavitation above liquidus. This mechanism includes improved wetting of solid particles, local undercooling upon the collapse of cavitation bubbles and pre-solidification of particles inside fine capillaries.

The main objectives of this fundamental research are as follows:

(1) Determine the dominant mechanisms for grain refinement under UST processing.

(2) Determine the relevant parameters of the UST processing.

(3) Investigate the as-cast microstructure and tensile properties of the UST processed material in conjunction with relatively low (e.g., silica sand molds) and high (e.g., permanent molds) cooling rates.

(4) Determine the feasibility of casting UST-processed materials at relatively high superheat; this will assist in scaling up of the ultrasonic technology for commercial applications.

The thesis is presented in the following sequence: chapter II provides a literature review, chapter III will present the experimental approach, chapter IV will present and discuss in detail the experimental results and chapter V will present the conclusions and recommended future work.

2.0 LITERATURE REVIEW

2.1 A356 ALLOY

Aluminum alloy A356 was selected as the metal we used because it is readily castable and widely studied and used. Typical A356 alloy is used to make aircraft pump parts, automotive transmission cases, aircraft fittings and control parts, water-cooled cylinder blocks and other applications where excellent castability and good weldability, pressure tightness, and good resistance to corrosion are required.

The chemical composition of the A356 alloy is shown in Table 1.

Table 1 Nominal chemical composition of matrix alloy A356

Element	Si	Fe	Cu	Mn	Mg	Zn	Ti	Al
wt. %	6.5-7.5	0.20	0.20	0.10	0.25-0.45	0.10	0.20	balance

2.2 NUCLEATION MECHANISMS:

Grain structure is principally affected by the nucleation rate [9; 13; 14; 59]. Basically, there are three mechanisms for nucleation: homogeneous, heterogeneous, and dynamic nucleation.

Homogeneous nucleation is dependent on the undercooling of the melt which is related to the cooling rate during solidification. Heterogeneous nucleation is influenced by the impurities in the melt and the addition of grain refiners. Dynamic nucleation is caused by dendrite fragmentation at the solidification front in essence.

2.2.1 HOMOGENEOUS NUCLEATION

Homogeneous nucleation is the formation of solids within the melt without the aid of foreign materials. Above or below the equilibrium transformation temperature, fluctuations in density, atomic configurations, heat content, etc., occur in the liquid. They make possible the formation of minute particles of crystalline solid (long range order), called embryos. Consequently, a liquid-solid interface is created, and associated with it is interface energy. As a result, the free energy of the system increases, and, unless sufficient undercooling is available, the embryo will remelt. If the undercooling of the melt is sufficient, the embryo will survive, and will grow to form a nucleus. Because the nucleus has the same composition as the liquid and solid, this is called homogeneous nucleation. It can be demonstrated that the embryo must grow to a certain critical size in order to become stable and form a nucleus.

Consider that an embryo of radius r is formed in the liquid. This will result in a change in free energy, firstly, because of the decrease in the free energy resulting from the change of the volume of radius r from liquid state to solid, and secondly, because of the increase in the free energy due to the newly created liquid-solid interface. The change in free energy is [26; 58]:

$$\Delta G = \frac{4}{3}\pi r^3 \Delta G_v + 4\pi r^2 \sigma \qquad (1)$$

where ΔG_v is the free energy per unit volume, and σ is the surface tension, or interfacial energy per unit area. The first term corresponds to the energy change due to the formation of solid phase in the supercooled liquid, and the second term shows the surface energy of the newly formed nuclei. The whole equation is represented by the ΔG curve in Fig. 1.

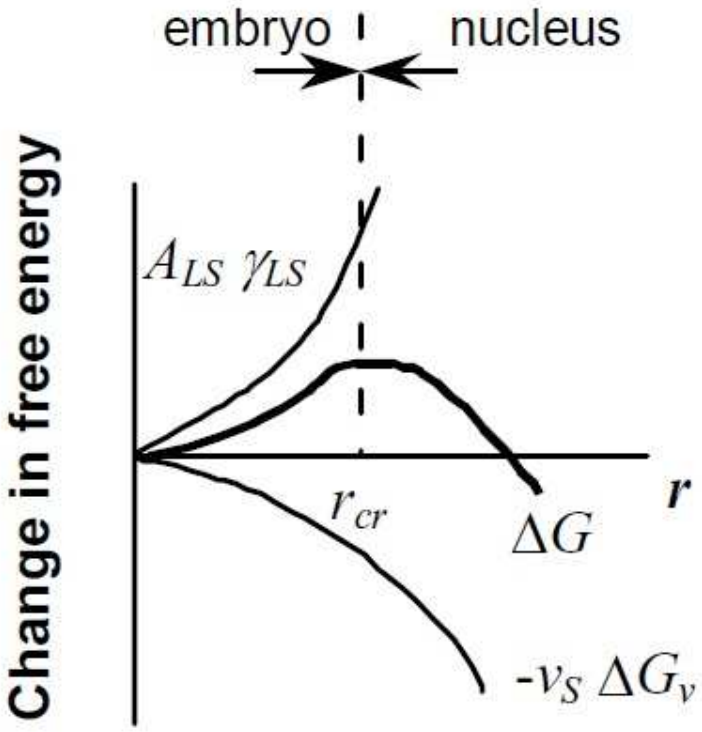

Fig. 1: Variation of the free energy of the liquid-solid system with the radius of the embryo [63].

Since theΔG must be negative for nucleation to occur, the critical radius of the nuclei is:

$$r^* = -\frac{2\sigma}{\Delta G_v} \tag{2}$$

The rate of homogeneous nucleation, which is a key parameter for determining the size of the grains in a solidified metal, is given by [58; 63]:

$$I(T) = \omega A \exp\left(\frac{\Delta G_m}{kT}\right) \exp\left(\frac{\Delta G^*}{kT}\right) \tag{3}$$

where ω is related to the atomic oscillation frequency, $\exp(\frac{\Delta G_m}{kT})$ represents the kinetics of atomic migration for the activation energy ΔG_m, and $\exp(\frac{\Delta G^*}{kT})$ is the volumetric energy of formation of stable nuclei. This balance between the kinetics of atomic migration and the thermodynamic driving force lead to a maximum nucleation rate at intermedial undercooling, see Fig. 2 [63].

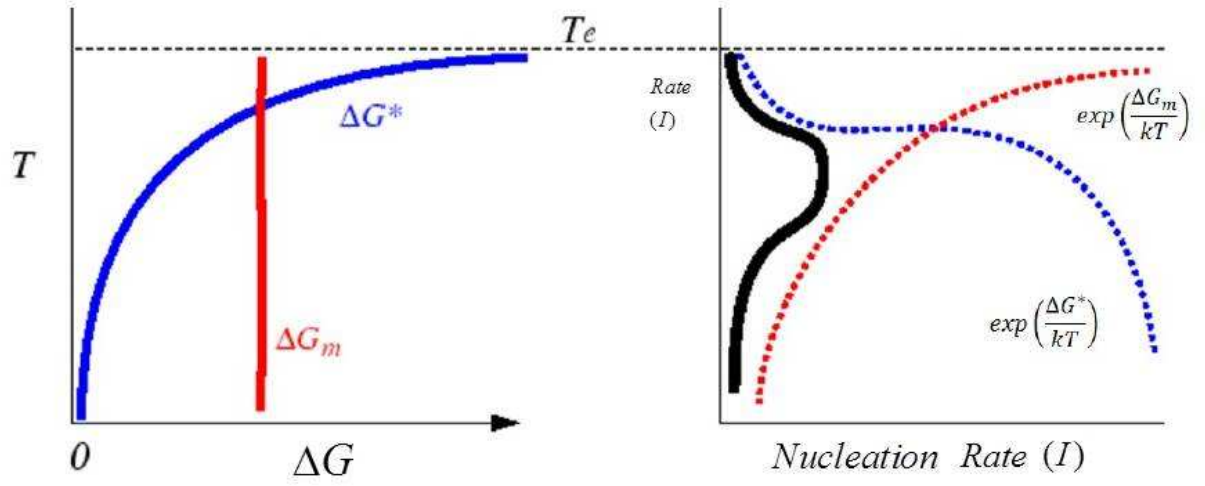

Fig. 2: Nucleation rate at Temperature T with respect toΔG_m and ΔG^*. [63]

2.2.2 HETEROGENEOUS NUCLEATION

Heterogeneous nucleation occurs more readily than homogeneous nucleation due to the lower energy requirement to form a nuclei on a solid surface [26; 58], such as impurities in the bulk liquid like intermetallics or at the walls of the casting mold, see Figure 3. The number of heterogeneous nuclei is directly related to the number of foreign solid phases in the liquid. There are several approaches to increase the rate of heterogeneous nucleation during solidification to

produce fine grain structures. These include inoculation of the liquid metal and fragmentation of dendrites by stirring [63].

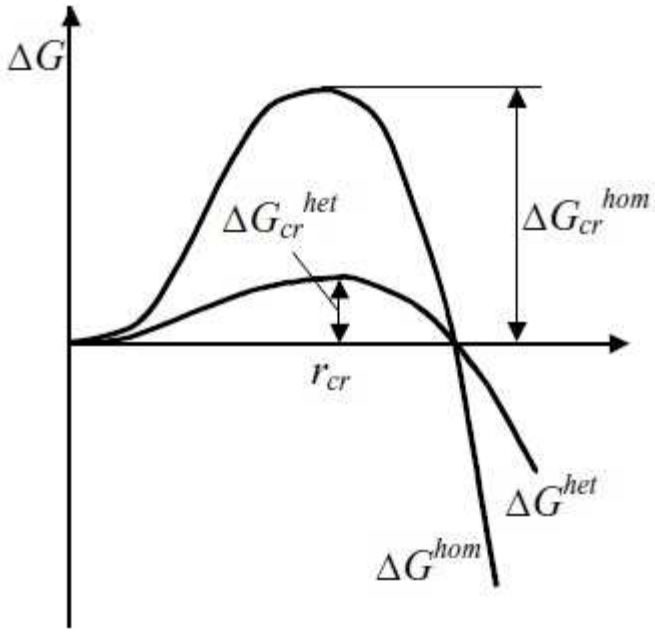

Fig. 3: Energy required for nucleation in a liquid [63].

2.2.3 DYNAMIC NUCLEATION

Dynamic nucleation refers to the formation of nuclei by the fragmentation of solidified grains. This is the basis for various grain refinement methods [15; 31; 40; 46; 47; 56; 68]. There are two proposed mechanisms: the big bang and convective crystal fragmentation mechanism [63]. The big bang mechanism explains the columnar to equiaxed transition during solidification. In this mechanism the columnar grains forming during the initial stages of solidification are fragmented by the ripening and local remelting of secondary arms. The

principle behind this mechanism is that as the solidifying material becomes more solute-rich, the melting point is lowered causing the trunks of dendrite tips to melt and be carried away by the fluid flow eventually acting as a new heterogeneous nucleation site. Experiments by Herlach et al. [15] based on Ni-Cu alloys showed this mechanism. The fragmentation was indicated by sphere-like particles in the wake of dendritic microstructures. This finding suggested that the undercooled melts initially formed a coarse dendritic structure and subsequent supersaturation of the alloying element at the dendrite trunk during growth caused the structure to subsequently fragment and form small equiaxed grains [15; 31; 40; 46; 47; 56; 68].

The second mechanism is caused by mechanical shear forces on the dendrite tips at the solidification front [8]. The shear forces are generated by the flow in the melt induced by mechanical or ultrasonic stirring. It was initially thought that fluid flow in the melt caused this mechanical fragmentation; however, studies by Paradies et al. [8] of the flow velocity on grain fragmentation revealed that the mechanism was actually due to the temperature and solute gradients generated by the fluid flow [8; 64]. While the solute rich regions are the mechanism for dendrite fragmentation, Campanella et al. [64] showed that in solute rich alloys the fragmentation occurs more readily than in solute lean alloys resulting from the density of the mushy zone in the melt and the permeability of the liquid in the dendritic structure. Later, it was suggested by Li et al. [40] that while for middle range undercooling the fragmentation was a result of solute entrapment, for large undercooling fragmentation was attributed to internal stresses from shrinkage during rapid solidification.

2.3 UST GRAIN REFINEMENT MECHANISMS

UST can apply high intensity of acoustic energy into the melt [19; 21; 60]. The application of ultrasonic energy to the melt causes instantaneous local pressure oscillation. During cavitation, low pressure creates tiny bubbles while high pressure makes the bubbles collapse and produce shock waves. During the solidification of castings, UST can be used for degassing and microstructure refinement and modification:

Cavitation involves the formation, growth, pulsating, and collapsing of tiny discontinuities or bubbles in liquid [1; 18; 44; 54]. The discontinuities result from the tensile stresses generated by the sound wave during the tensile phase. If the tensile stresses persist once the bubble has been formed (negative sonic pressure or tension), the bubble will expand and may be several times bigger than its initial size. The cavitation bubble is initiated and moves in liquid simultaneously with many other bubbles spaced by less than one wavelength and forming a cavitation region.

It is supposed that acoustic cavitation in liquids develops according to a chain reaction. Therefore, individual cavities are developing so rapidly that within a few microseconds the active cavitation region is created close to the source of the ultrasound power [28].

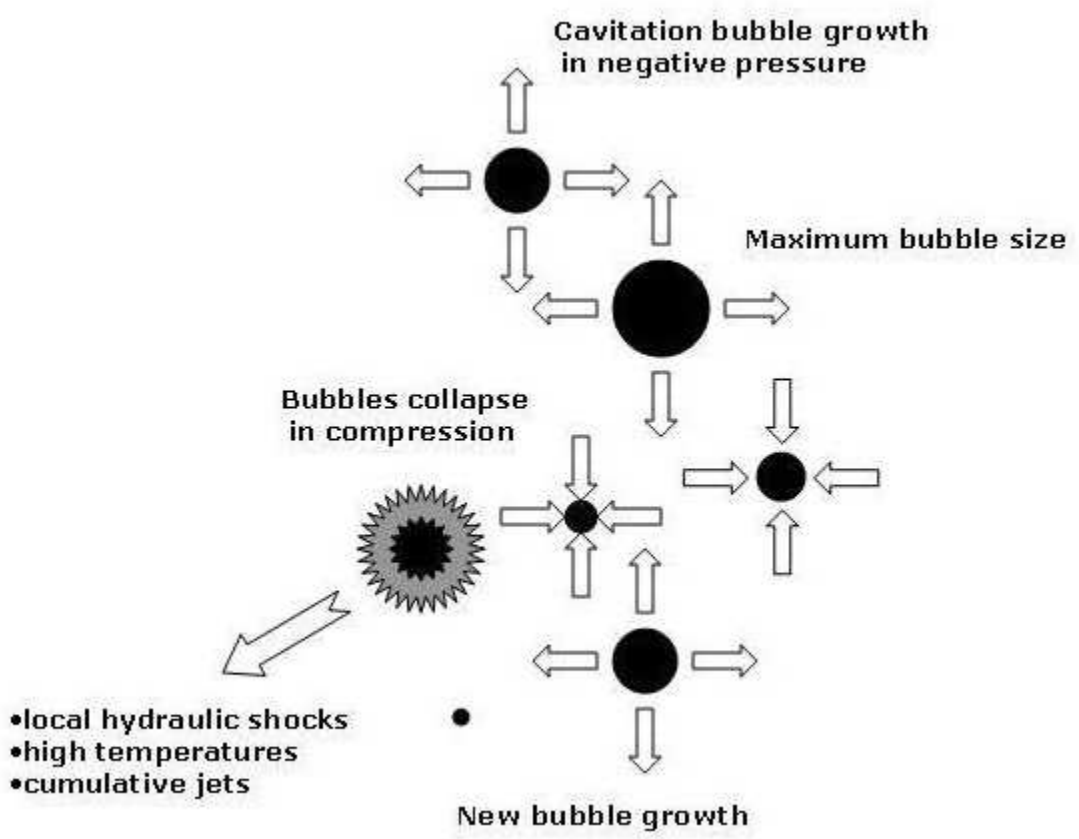

Fig. 4: Schematic image of cavitation bubble pulsation with collapse [23].

The bubble, in fact, can pulse, either linearly or nonlinearly, with respect to its equilibrium radius, or it can increase to a maximum size and then begin to collapse until the rapid rise in pressure inside the cavity prevents further motion. Before bubbles reach their maximum size they accumulate the ultrasonic energy over several pulsation periods (100 to 200 x 10-6 s) [29]. Upon the collapse of these bubbles, high temperatures (up to 1000 °C), pressures (tens of thousands of MPa [20]), and other forces, such as micro-jetting, turbulence, acoustic streaming, etc., are generated. These physical effects are suggested as possible mechanisms for ultrasonic cleaning, degassing, melt filtration, grain refinement, semi-solid processing, production of natural composites based on aluminum, etc. [10; 35; 43; 48].

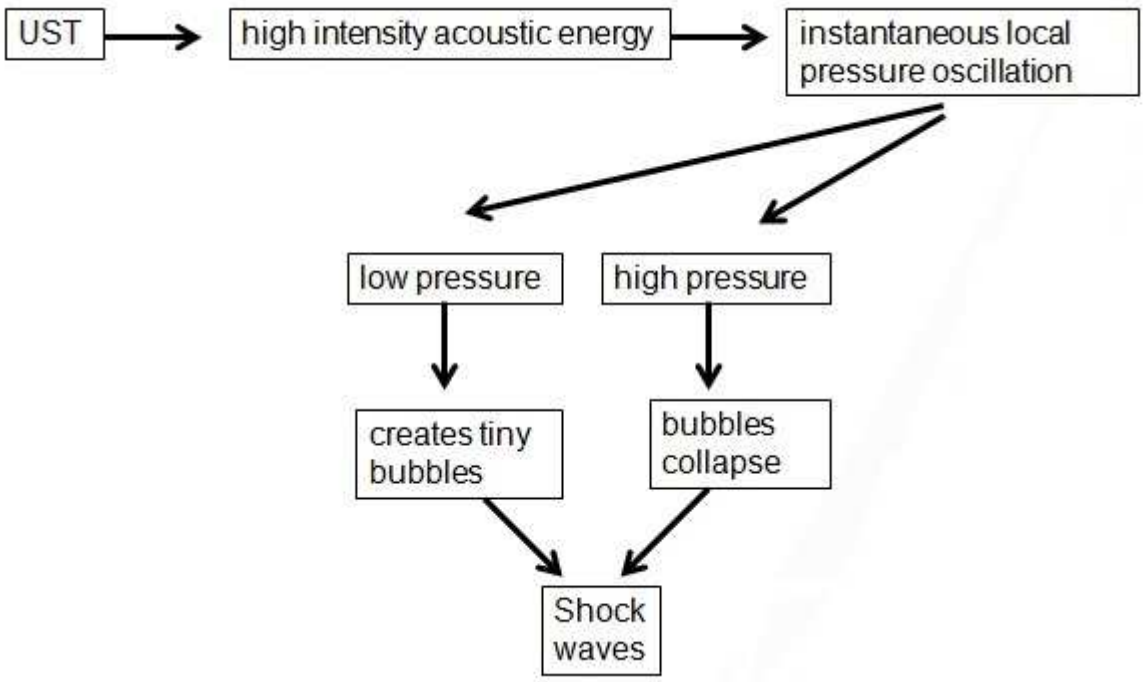

Fig. 5: Phenomena occur in the melt during the UST processing.

The main effects of the UST processing are:

(1) UST induced degassing: During the cavitation process, very small bubbles are created at low pressure. These bubbles can act as nuclei for the formation of hydrogen and vapor bubbles. Hydrogen will escape from the liquid. The degassing efficiency is proportional to the ultrasonic intensity [36].

(2) Grain nucleation: There are several ways that UST can alter grain nucleation [42]. Since the pressure oscillations exist in a melt under UST processing, the liquidus temperature for the melt is changed. Thus, some part of the melt is superheated and the other part is undercooled. This phenomenon occurs at high frequencies and causes increase in the amount of nuclei into the melt.

(3) Dendrite fragmentation: Dendrites usually start melting at the root due to local temperature rise and segregation. In the melt, UST produces strong convection and shock waves which may promote dendrite fragmentation. Convection can promote dendrite fragmentation because it causes local temperature and composition variations and promotes diffusion of solute. Shock waves will induce the breakage of the melting root [15; 33; 46; 61; 69].

The mechanisms for UST induced grain refinement are related to pressure and temperature oscillations in the melt. As previously discussed, these oscillations are likely to induce heterogeneous nucleation in the melt. In addition, they are probably enhancing dendrite fragmentation. However, the dominant mechanism for grain refinement has not yet been determined. More related experiments need to be performed to understand which mechanism is dominant.

There have been many different views regarding the mechanisms of ultrasonic grain refinement. Generally these mechanisms can be classified into two groups due to the absence and presence of cavitation. In the first group, they share the same assumption that grain refinement is induced by ultrasonic under the frequency below the cavitation threshold. In this group, there are also two different views. Chernov [16] holds the view that a strong stirring effect exists in the melt because of the UST. The strong stirring effect will significantly increase the heat transfer from the melt to the environment, therefore the melt is cooled down and the nucleation is enhanced. This stirring effect can be achieved by mechanical stirring and other methods. By measuring the temperature in the melt, the cooling down of the melt can be observed.

Abramov came up with a new theory [2]. By using UST under a frequency below the cavitation threshold, Abramov conducted some experiments to disperse organic and metallic crystals. It was observed that the UST under the frequency below the cavitation threshold had no significant effect on the solidification front; only the temperature distribution in the melt had been changed. By using the UST treatment of the melt, a wide two-phase zone is formed to promote grain refinement, even in the absence of cavitation in the melt. The refinement is affected by G/V ratio (G is the temperature gradient and V is the solidification rate). Increasing the temperature gradient and decreasing the solidification rate would cause less grain refinement. Abramov explains that the ultrasonic treatment using a frequency below the cavitation threshold may result in pressure oscillations, viscous friction forces and dynamic forces, which promote the grain refinement.

In the second group, one explanation for cavitation-aided grain refinement [7; 55; 57; 65] is about shock waves. UST causes pressure oscillations. Low pressure produces tiny bubbles. When the bubbles collapse, powerful shock waves are generated. It is believed that shock waves occurring near the solidification front cause dendrite fragmentation. Therefore, dendrite fragments may act as nucleation sites [24; 62]. This opinion also assumed that cavitation can activate inclusions in the melt to turn to nucleation sites. Those inclusions are usually unwettable by metal melt, but under the UST treatment, bubbles may form on those inclusion particles which make them to be wettable [22-24].

Another mechanism of grain refinement in the presence of cavitation was proposed by Chalmers [12]. The pressure increase leads to rise of solidification temperature, which promotes nucleation in the melt. Assuming that the local pressure will rise to 100 – 1000 MPa, the melting

point of aluminum can temporarily increase by more than ten degrees. Therefore, the undercooling in the melt can be increased enough to enhance nucleation.

Hem [37] proposed another mechanism. During the expansion process, the bubbles size increase rapidly. At the same time, the liquid evaporates inside the bubble. The expansion and vaporization will reduce the bubble temperature. As long as the temperature keeps falling down below the solidification temperature, certain amount of undercooling is formed to enhance the nucleation on the bubbles. Although large amount of effort has been put in the field of ultrasonic processing of metal, the mechanism of UST induced grain refinement has not yet been determined. This means that additional experimental work still needs to be performed to clearly understand which mechanism is dominant for UST induced grain refinement.

2.4 MODELING OF ULTRASONIC CAVITATION:

A comprehensive multi-phase ultrasonic cavitation model was developed by Nastac [50-53]. In this modeling approach, a basic two-phase cavitation model was used that consists of using the standard viscous flow equations governing the transport of phases (Eulerian multi-phase) and the k-□ turbulence model. In the cavitation domain, the liquid-bubble mass transfer was shown to be governed by the cavity (bubble) transport equation:

$$\frac{\partial}{\partial t}\left(f_b\ \rho_b\right) + \nabla \cdot \left(f_b\ \rho_b\ \vec{V}_b\right) = R_G - R_C \qquad (4)$$

Where *b* subscript denotes the cavitation bubble phase, f_b is the bubble volume fraction, □$_b$ is the bubble density, $\vec{V}_b$ is the bubble phase velocity, R_G and R_C are the mass transfer source terms

related to the growth and collapse of the cavitation bubbles, respectively. In Eq. (4), the interphase mass transfer rates per unit volume (R_G and R_C) account for the liquid and bubble phases in cavitation. They are calculated using the growth of a single bubble based on the Rayleigh-Pleasset model. The Rayleigh-Pleasset model assumes no barrier for nucleation; thus, the bubble dynamics can be calculated from the Rayleigh-Plesset equation (5):

$$R_b \frac{d^2 R_b}{dt^2} + \frac{3}{2}\left(\frac{dR_b}{dt}\right)^2 = \frac{p_b - p}{\rho_L} - \frac{2\,\sigma_L}{\rho_L\, R_b} - \frac{4\,\nu_L}{R_b}\frac{dR_b}{dt} \qquad (5)$$

Where R_b is the bubble radius, σ_L is the surface tension coefficient of the liquid phase, ρ_L is the liquid density, ν_L is the kinematic viscosity of the liquid phase, p_b is the bubble surface pressure, and p is the local far-field pressure.

A simulation example is presented below for the Figure 6 shows the geometry of the liquid pool used in the ultrasonic analysis. In Figure 6, the ultrasonic probe has a diameter of 20 mm, an amplitude, A = 10 microns, and a resonant frequency, f = 17.5 kHz. The flow field and cavitation region profiles are shown for two different times in Figs. 7 and 8, respectively. Fig. 8 shows that the predicted ultrasonic cavitation region is relatively small; hovewer the acoustic streaming is strong and thus the created/survived bubbles/nuclei can be transported into the bulk liquid quickly.

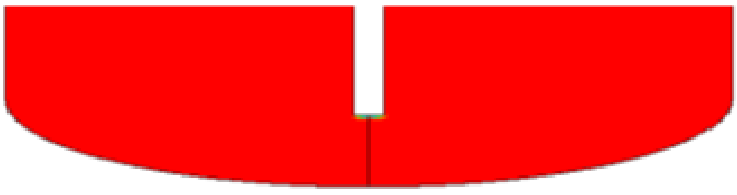

Fig. 6: A356 liquid pool (the ultrasound probe is shown in the middle of the pool) [52].

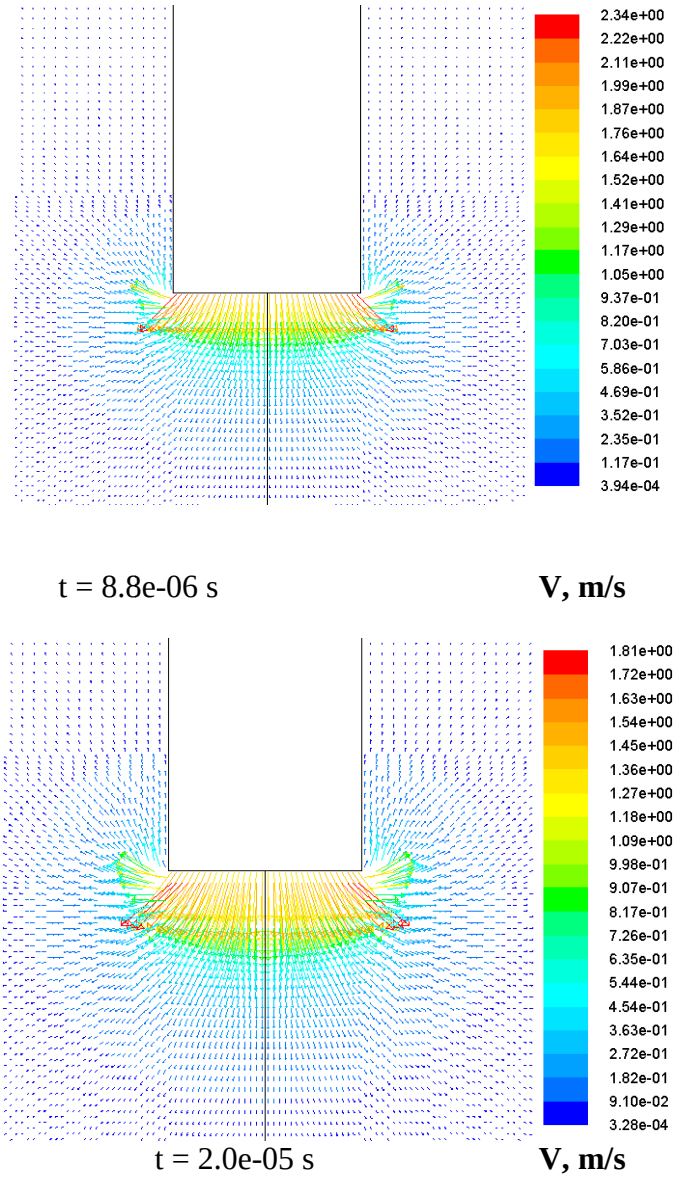

Fig. 7: Flow induced by ultrasound: Flow field (velocity vector) [51; 52].

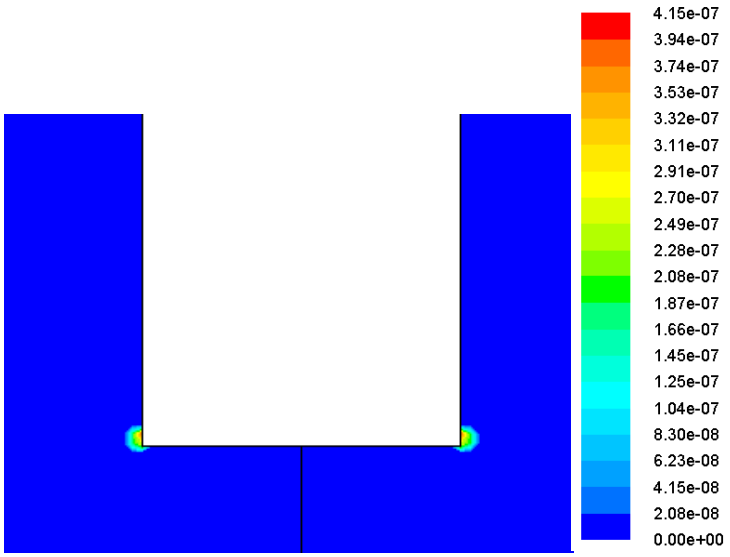

(a) t = 8.8e-06 s

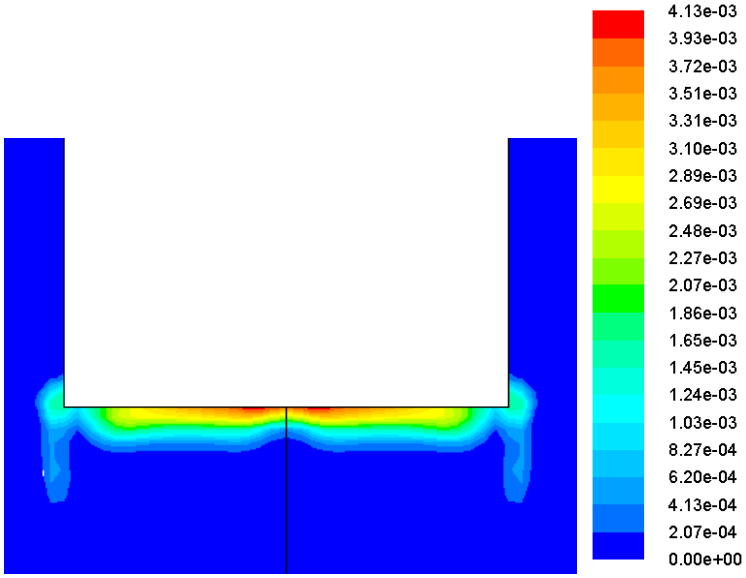

(b) t = 2.0e-05 s

Fig. 8: Cavitation induced by ultrasound. Legends show the volume fraction of cavities/bubbles/potential nuclei (cavitation region) [51; 52].

Figure 9 show the predicted microstructure in the presence of UST. The stochastic mesoscopic model developed by Nastac [50; 53] was used to study the ultrasonic stirring effects on the grain refinement of commercial alloys. The microstructure model includes calculations of the grain size, columnar-to-equiaxed transition (CET) and of segregation. In Fig. 9 it is shown that the predicted grain size under UST processing is approximately one order of magnitude lower than that without UST.

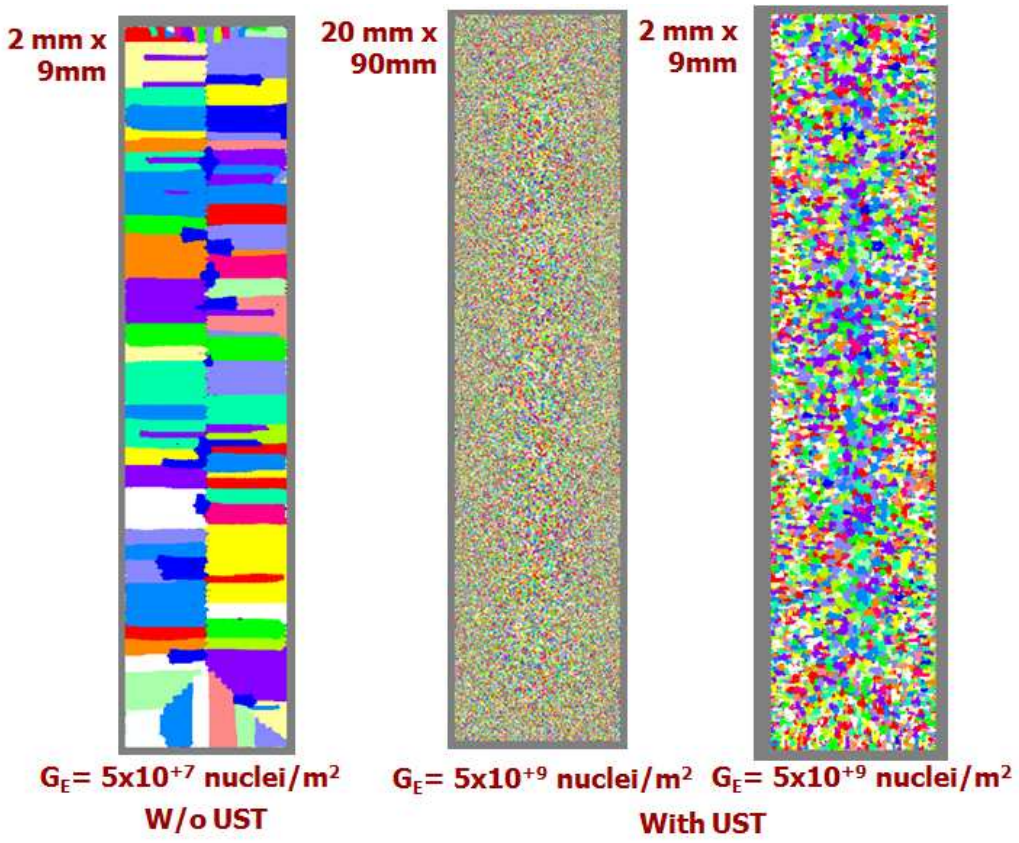

Fig. 9: Ultrasonic Treatment: Prediction of Microstructure [50; 53].

3.0 EXPERIMENTAL APPROACH

3.1 EXPERIMENT SETUP

A sketch of the UST treatment equipment is presented in Fig. 10. More details are shown in Fig. 11. The setup consists of an 18 kHz 4 kW ultrasonic generator, a transducer, a cylindrical Nb probe (4 cm diameter), a control panel (for power and frequency adjustments) and an induction furnace that is used to melt the A356 alloy. The position of the ultrasonic probe can be adjustable. The melt temperature is measured by a K-type thermocouple. Electro-nite (http://heraeus-electro-nite.com/en/home/home_1.aspx) pouring cups were used to obtain cooling curves under different process conditions. The equipment presented in Figs. 10 and 11 was custom built to perform the present UST study.

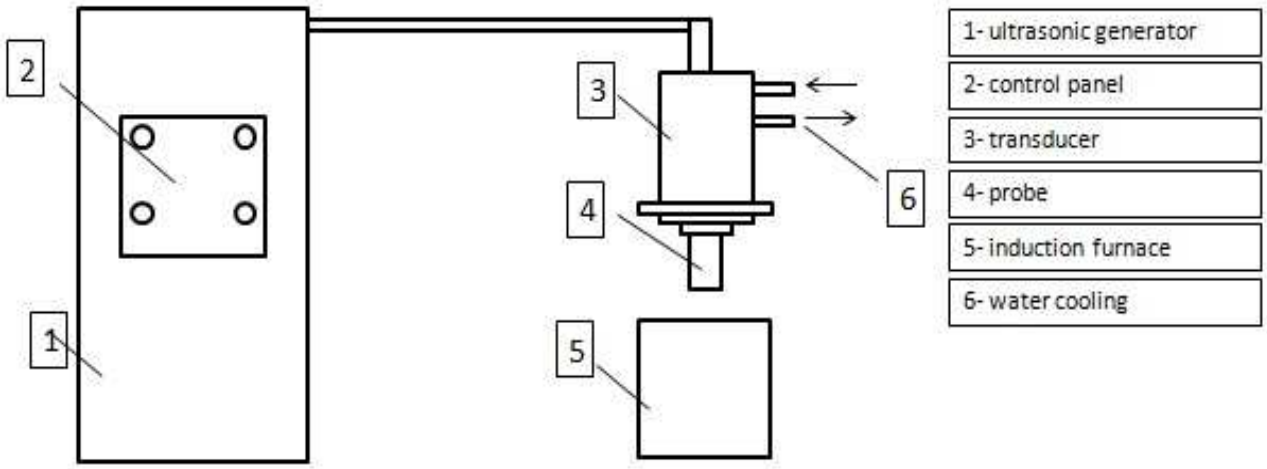

Fig. 10: Schematic of the UST system.

Fig. 11c illustrates the permanent metal mold, which is an ASTM B108-02 standard mold. The mold can be preheated in a controlled manner from room temperature to a maximum temperature of about 400 °C. Approximately 3 lb (1.4 kg) of A356 alloy is needed to fill the mold. Two tensile test bars are obtained from a casting.

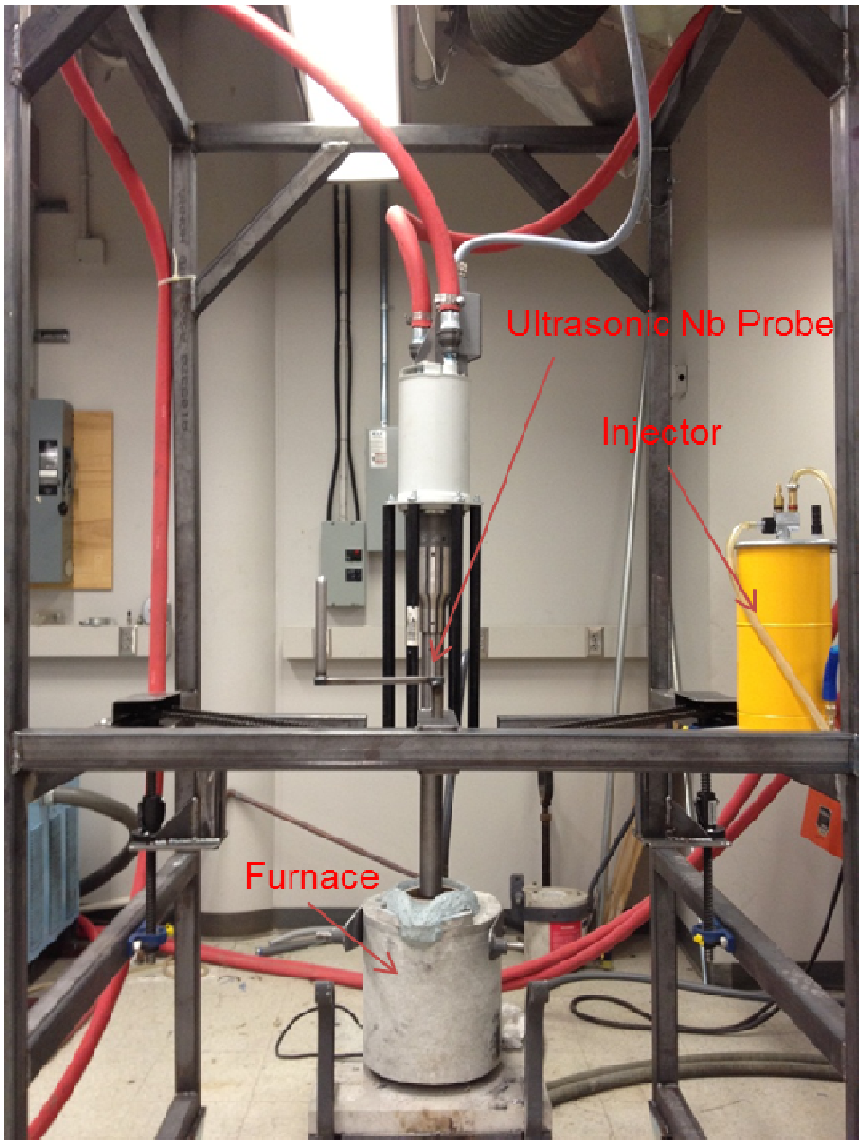

(a)

Fig. 11: Detailed UST system: (a) Ultrasonic probe; (b) ultrasonic generator; and (c) permanent mold

(b)

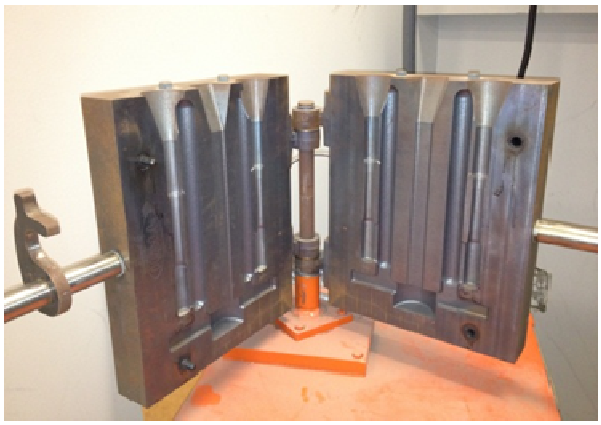

(c)

Fig. 11 continued: Detailed UST system: (a) Ultrasonic probe; (b) ultrasonic generator; and (c) permanent mold.

3.2 EXPERIMENT PROCEDURE

The experimental procedure consists of the following sets of experiments:

Experiment 1A: Firstly, the furnace was heated up to 1382°F (750°C) to melt the A356 ingot material. Then the ultrasonic probe was inserted about 2 in. (5.1 cm) into the melt. A 1.75 kW power (about 70% of the maximum available power 2.4 kW) was applied to the melt via a Nb probe for 15 min. The melt surface was protected by argon. The melt was then poured into a ladle which has a capacity of approximately 10 lb (4.5 kg) and then from the ladle to a permanent metal mold which was preheated to about 800°F (427°C). The pouring temperature

of the melt was about 1382°F (750°C). After cooling down, the mold was removed and samples were prepared for metallographic characterization and tensile testing.

Experiment 1B: Similar conditions as in experiment A but after the UST treatment, the processed melt was poured into a pouring cup mold that was made of silica sand. The pouring cup was used to obtain samples at lower cooling rate.

Experiment 2A: The non-UST samples were obtained by Ar melt degassing at 1382°F (750°C) for 15 min, and then melt was poured into the permanent metal mold at 750°C (about 140°C superheat).

Experiment 2B: Similar conditions as in experiment C but the processed melt was poured into a pouring cup mold that was made of silica sand. The pouring cup was used to obtain samples at lower cooling rate.

Experiment 3A: Similar conditions as in experiment A but the UST treatment duration was 20 min.

Experiment 3B: Similar conditions as in experiment A but the UST treatment l duration was 5 min.

Experiment 3C: Similar conditions as in experiment A but the UST treatment duration was 1 min.

Experiment 4A: Similar conditions as in experiment A but the permanent metal mold was preheated to about 600°F (315°C).

Experiment 4B: Similar conditions as in experiment A but the permanent metal mold was preheated to about 400°F (205°C).

In each experiment, four small samples from the same position of cast samples were prepared for metallographic characterization and four tensile test bars were made to determine the tensile properties.

Notes:

(i) The experiments shown above were repeated at least twice to ensure the validity of the results.

(ii) The optimum application time of the UST processing (*e.g.*, 15 min) was established by performing several experiments by varying the UST application time as follows: 1 min, 5 min, 15 min, and 20 min. There no significant improvements when the UST processing time was exceeding 15 min. Accordingly, the optimum UST processing time was chosen to be 15 min.

(iii) The melt was also fully degassed by using the UST treatment

(iv) The pouring temperature used in all experiments was relatively high (*e.g.*, 750°C). The high superheat (about 140°C) of the A356 alloy was required to transfer the molten alloy from the furnace to the ladle and then completely fill up the permanent mold.

4.0 RESULTS AND DISCUSSION

4.1 MICROSTRUCTURE ANALYSIS

Experiments A-D:

Fig. 12a and 12b show the microstructures of A356 as cast without (experiment C) and with (experiment A) UST processing at the 200x magnification (M), while Figs. 12c and 12d show the same A356 as-cast microstructures at 1000x magnification. The samples without UST treatment have dendritic microstructure with larger secondary arm spacing than the ones with UST. It can be seen from Fig. 12b that the columnar dendritic structure was broken up because of the UST treatment. Basically, more equiaxed dendritic structure can be observed in the micrographs obtained via UST. When comparing Figs. 12c and 12d, it can be seen that the Si eutectic structure (black area) is more modified. This is another important effect of UST.

Fig. 13 illustrates the microstructure of the non-UST (experiment B) and UST processed (experiment D) samples solidified in the pouring cups (silica sand molds). The microstructures (in particular, the silicon phase) processed under UST are more modified when compared with the standard A356 alloy. When comparing Figs. 13a and 13b, it can be seen that the amount of porosity decreases. This is due to the ultrasonic induced degassing effect. Some related research studies shows that ultrasonic vibration can be used to reduce gas porosity formation in aluminum alloys. It can also be observed that the ultrasonic induced degassing is much more efficient than the Argon gas degassing (non-UST samples in Fig. 13a). Also, ultrasonic treatment can reduce the size of eutectic silicon by an order of magnitude; the aspect ratio was also reduced by ultrasonic treatment.

It can also be observed by comparing Figs. 12 and 13 that the microstructure size is significantly affected by both the cooling rate and the UST processing. The grain refinement effect in microstructures of sand mold samples is less evident than the effect in the microstructure of metal mold samples. This might be due to the fading of the UST grain refinement effect, which needs to be further investigated.

Table 2 presents the measured SDAS (secondary dendrite arm spacing) and eutectic spacing. The SDAS and eutectic spacing were measured from the micrographs. According to Table 2, the samples with ultrasonic treatment have both the SDAS and the eutectic spacing decreased by 15-20 %.

The decrease in eutectic spacing is usually due to high growth rates of these eutectic phases [27; 41]. But because high power acoustic energy was injected into the melt, slower growth rate of the eutectic phases may occur. Other phenomena that occur during ultrasonic processing of alloy may contribute to the refinement of the eutectic silicon phase. One phenomenon is the ultrasonic induced convection. The strong convection may enhance the heat transfer from the melt to the environment, which will definitely increase the cooling rate of the melt. Because of that, samples treated by UST may have higher eutectic growth rate. Acoustically induced convection can also affect nucleation of the silicon phases by altering the constitutional supercooling at the front of the growing eutectic grains.

Another phenomenon is the ultrasonic induced pressure oscillations in the liquid pools. Further research is still needed to determine the effect of this phenomenon on the growth of Si eutectic.

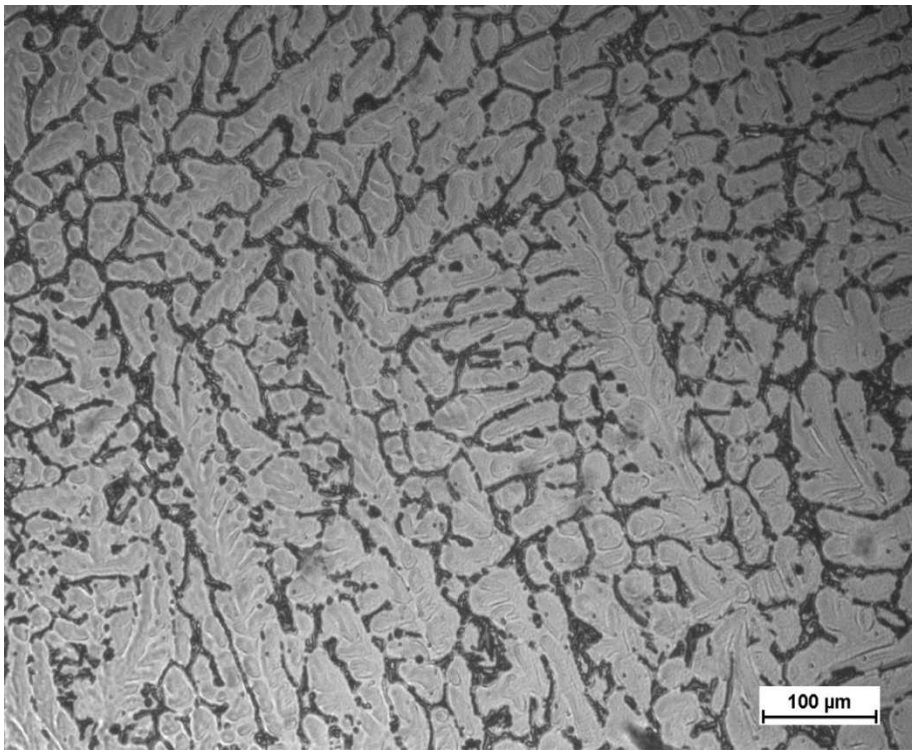

(a) Without UST; M= 200X.

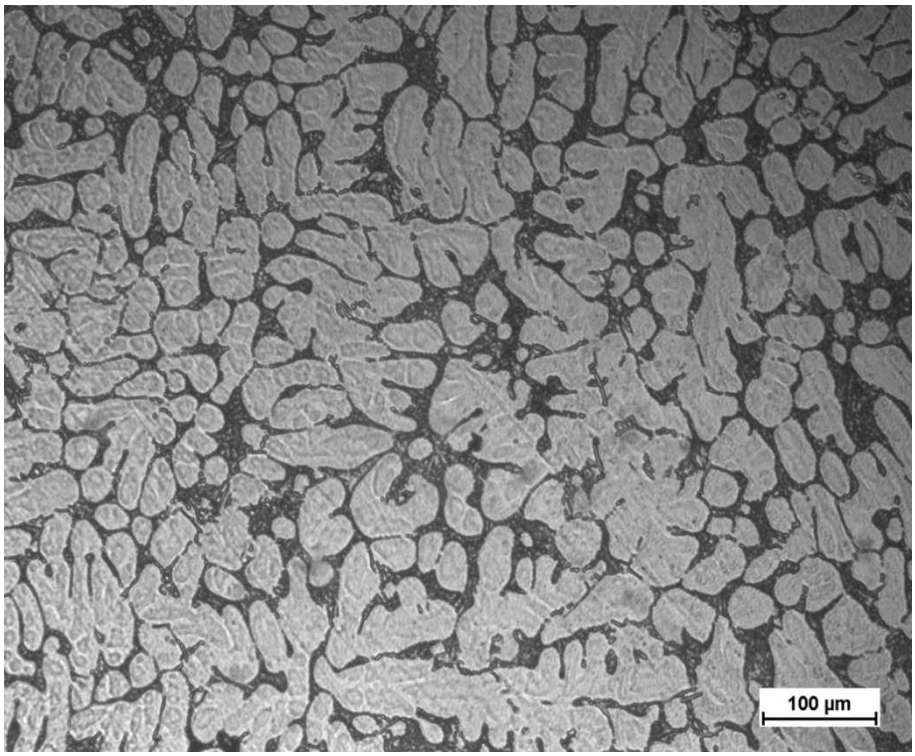

(b) With 15 min UST treatment; M= 200X.

Fig. 12: Micrographs of A356 permanent mold samples.

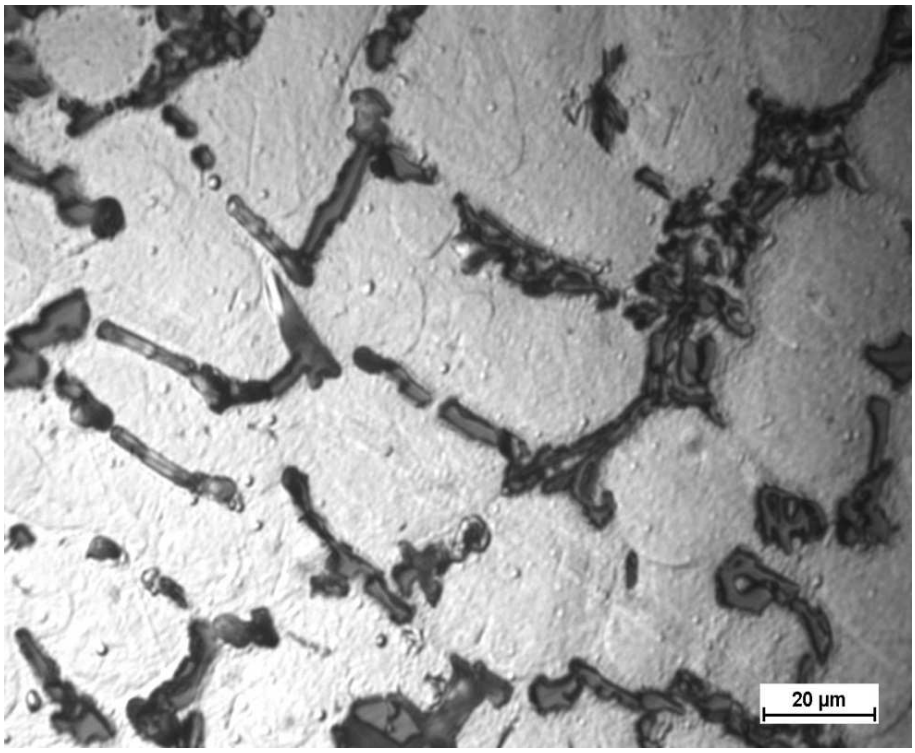

(c) Without UST; M=1000X.

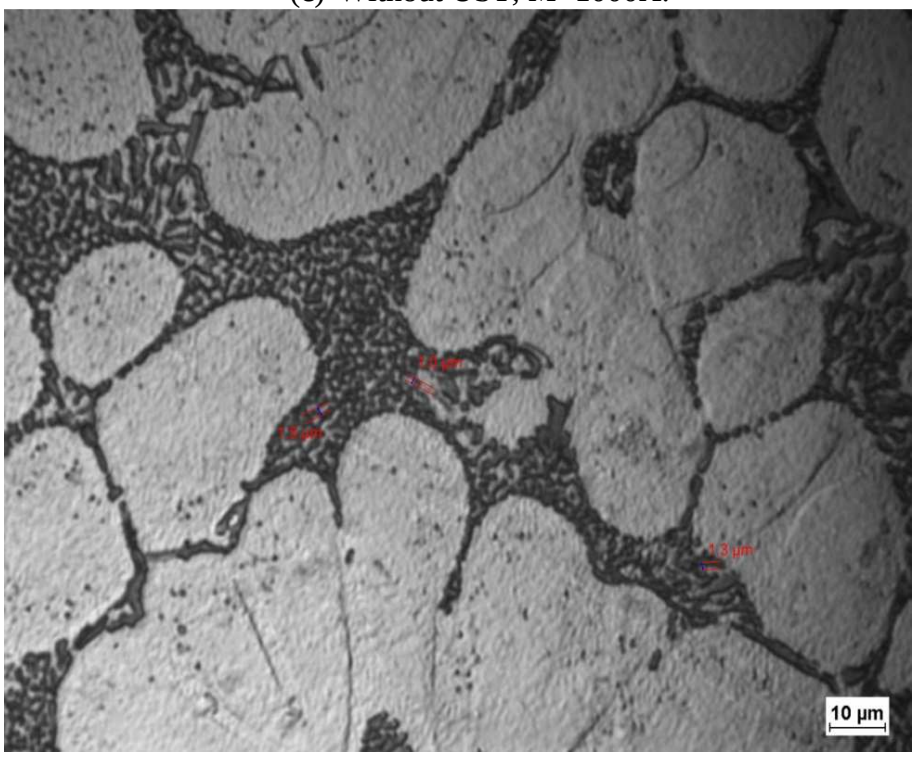

(d) With 15 min UST treatment; M= 1000X.

Fig. 12 continued: Micrographs of A356 permanent mold samples.

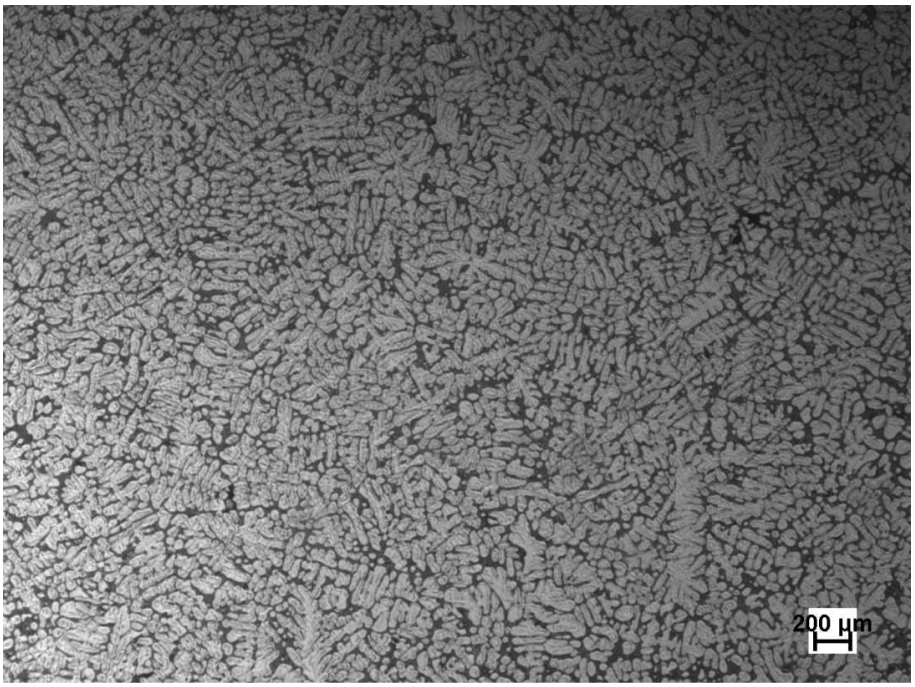

(e) With 15 min UST treatment magnified 50X

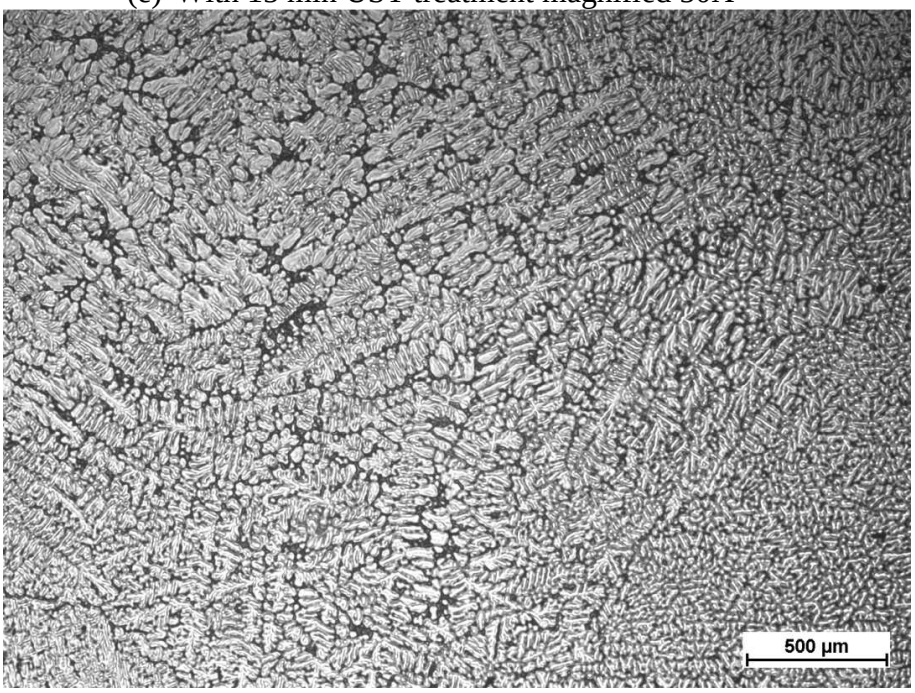

(f) Without UST; M=50X

Fig. 12 continued: Micrographs of A356 permanent mold samples.

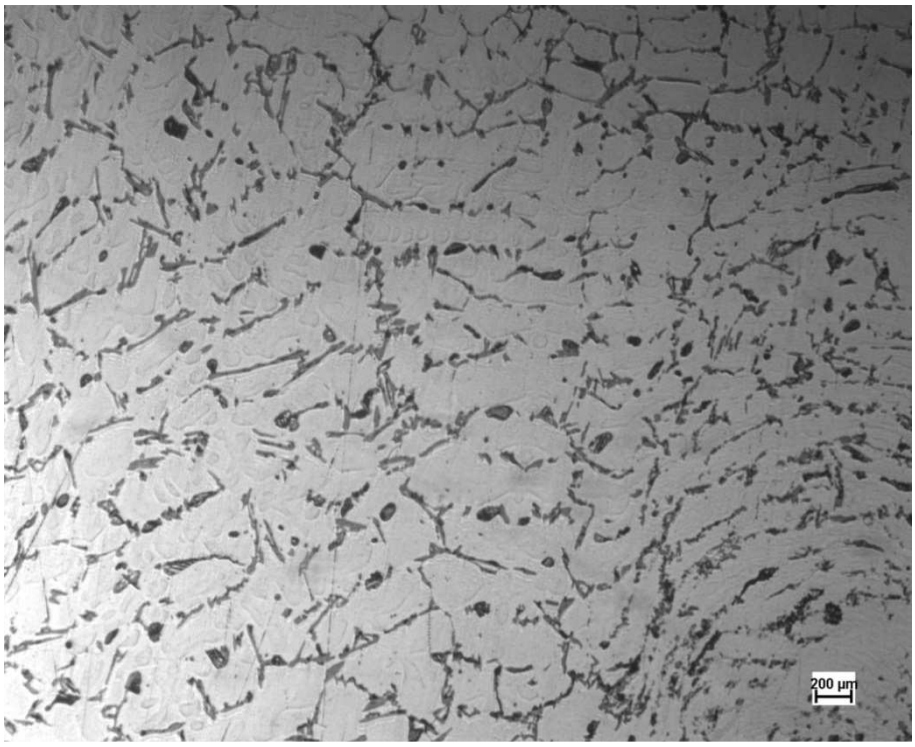

(a) Without UST; M=50X

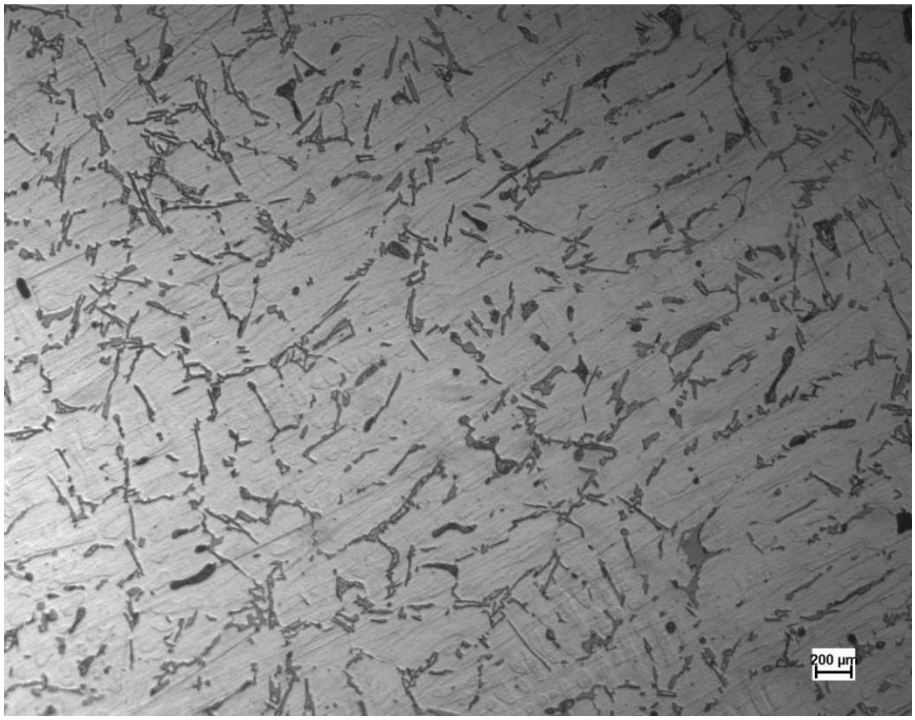

(b) With 15 min UST treatment; M=50X

Fig. 13: Micrographs of A356 silica sand pouring cup mold samples.

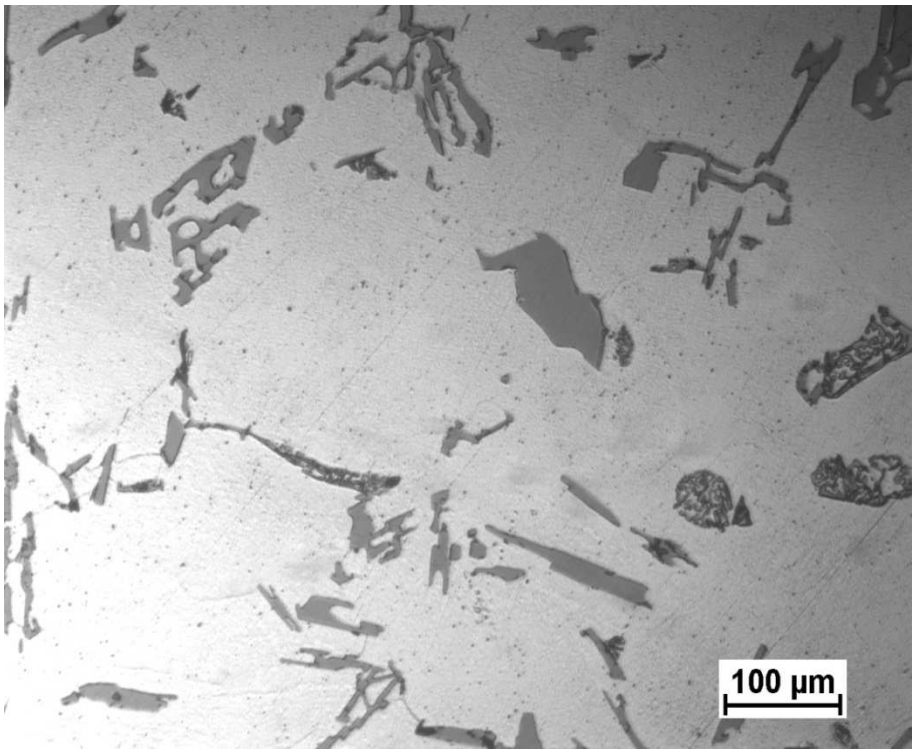

(c) Without UST; M=200X

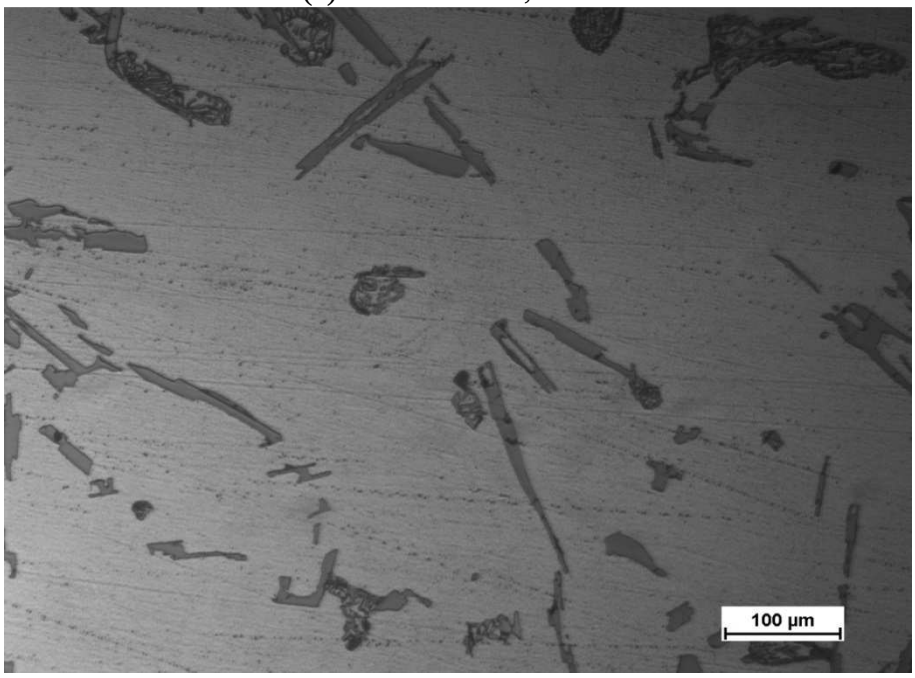

(d) With 15min UST treatment; M= 200X

Fig. 13 continued: Micrographs of A356 silica sand pouring cup mold samples.

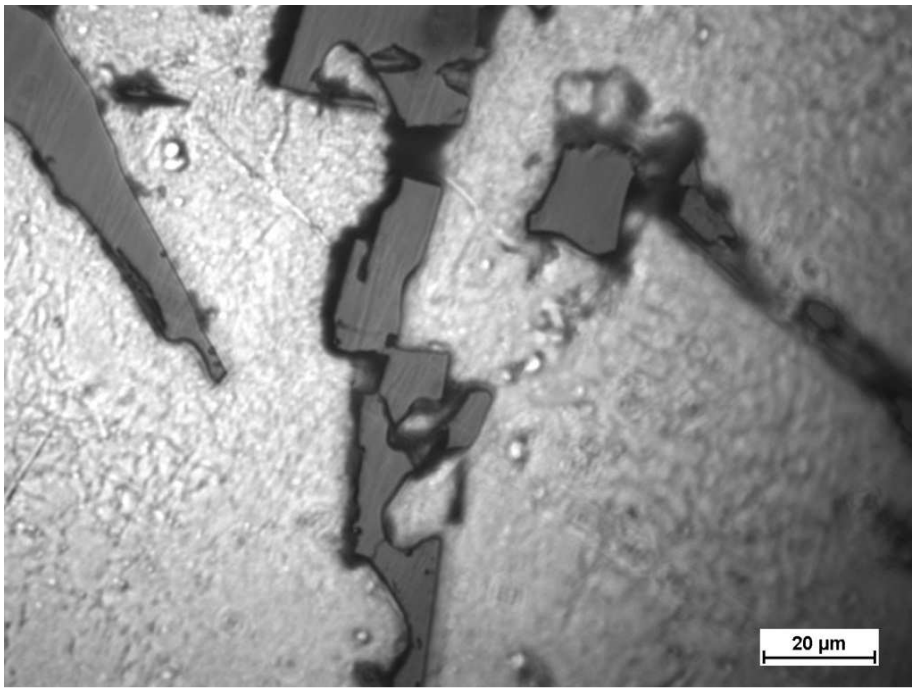

(e) Without UST; M=1000X

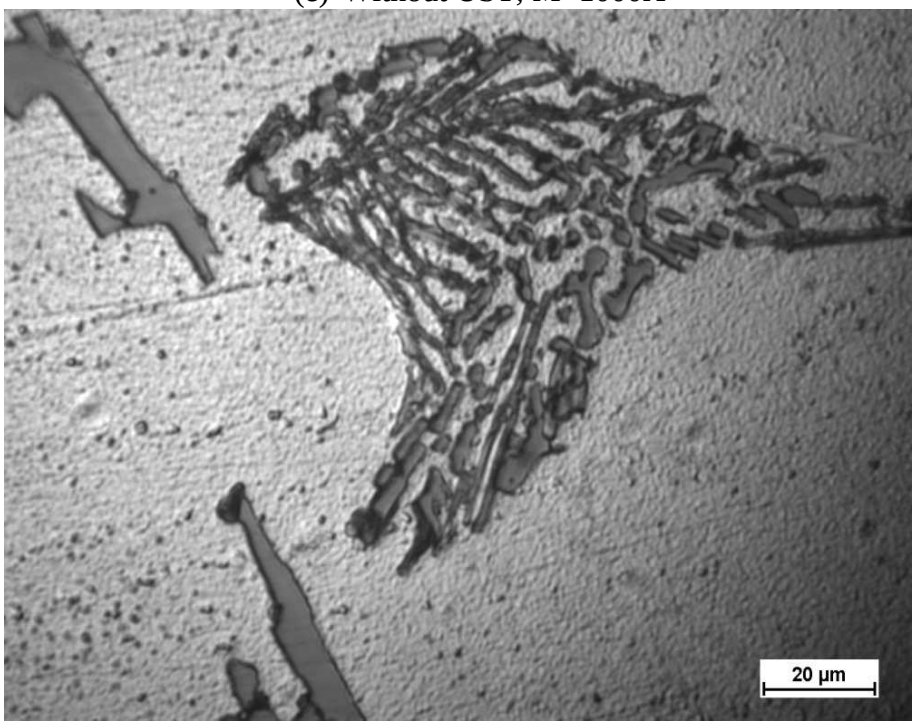

(f) With 15 min UST treatment; M= 1000X

Fig. 13 continued: Micrographs of A356 silica sand pouring cup mold samples.

Table 2 SDAS and Eutectic Spacing

Permanent mold samples	SDAS μm	Average μm	Eutectic spacing μm	Average μm
Without UST	26.5	28.9	1.8	2.1
	26.9		2.4	
	33.4		2.1	
15min UST	19.8	24.7	1.5	1.7
	23.0		1.6	
	31.4		1.9	

The effect of UST processing time: Figure 14 shows a comparison of microstructures obtained with different UST treatment durations, specifically 1 min, 5 min and 15 min. The samples treated for 1 min (Figs. 14 a and b) show excessive columnar dendritic morphologies implying that the UST processing time is insufficient. Figs. 14 c and d show the micrographs of the samples treated for 5 min. They still exhibit columnar structures. When the samples were treated for 15 min, the columnar structure was inexistent (Fig. 14 e). One of the explanation is the cavitations are just formed in the regions which are closer to the ultrasonic probe, they can diffuse into the bulk by fluid flow, but 1min and 5min are not enough to make cavitations sufficiently diffused.

The effect of the mold temperature: Fig. 15 describes the influence of the mold temperature (Tm) on the grain morphology of alloy A356. Three different mold temperatures were studied: 400 °F (204 °C), 600 °F (315 °C), and 800 °F (426 °C). It is observed that the sample processed at the lowest mold temperature (Fig. 15 a) has finer grain structure than the ones processed at higher temperatures (see Figs. 15 b and c). The samples processed at higher mold temperatures (Figs. 15 b and c) show similar grain morphologies.

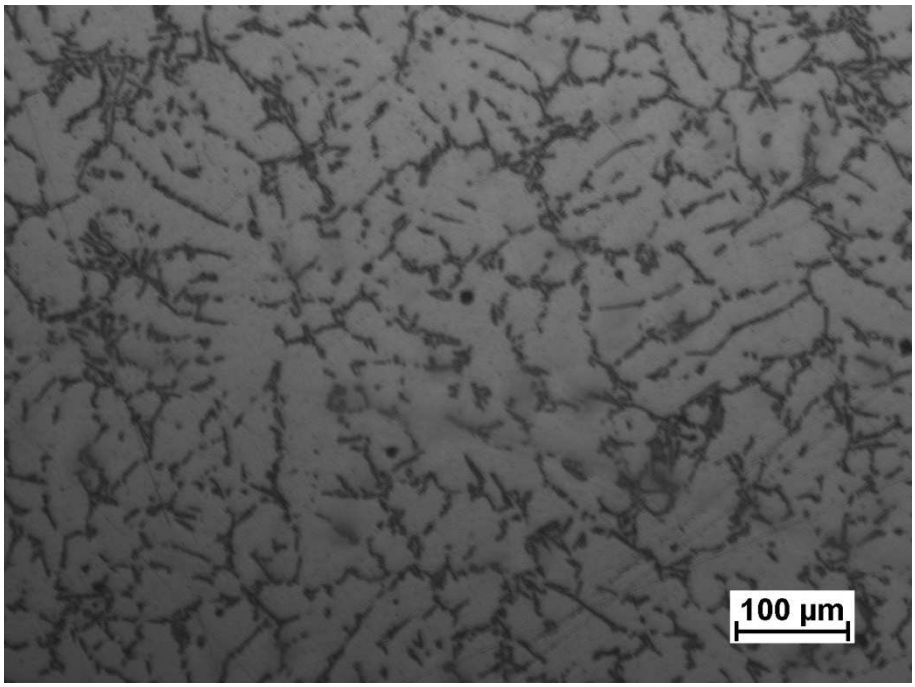

(a) 1 min; M=200X

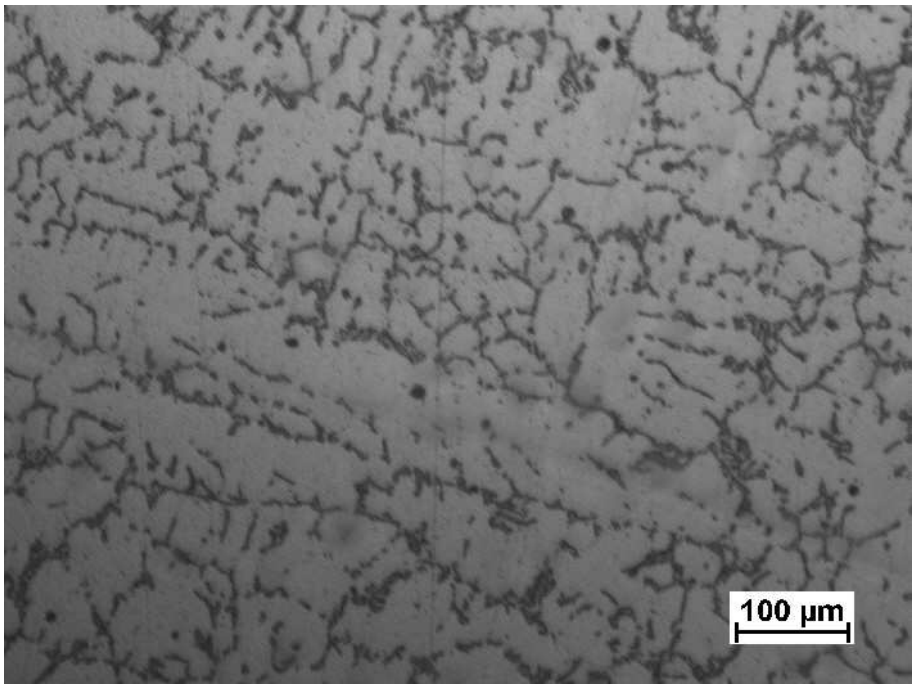

(b) 1 min UST; M=200X

Fig. 14: Microstructure comparison between samples obtained with different UST durations.

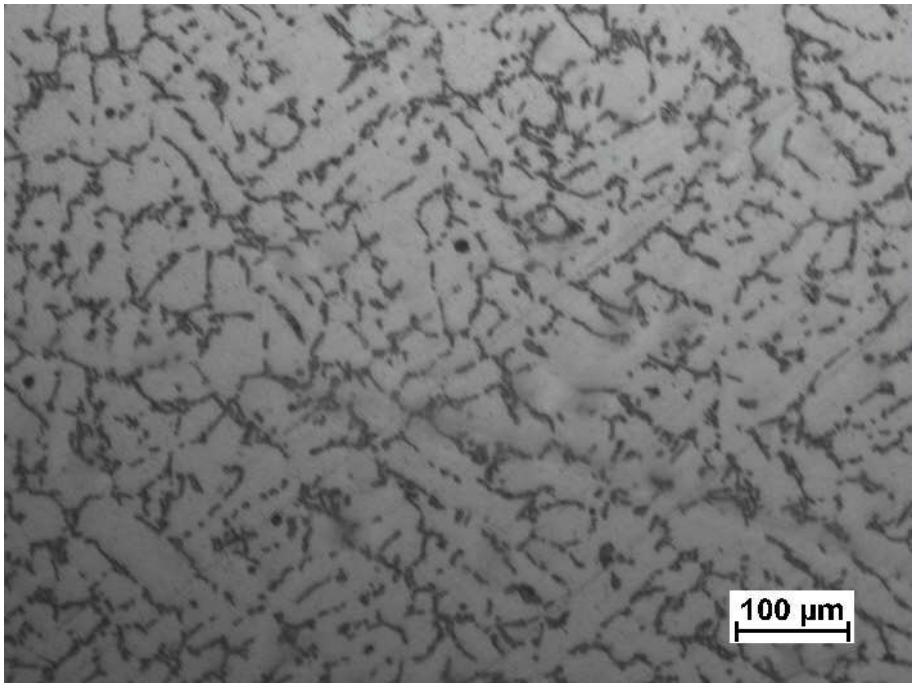

(c) 5 min UST; M=200X

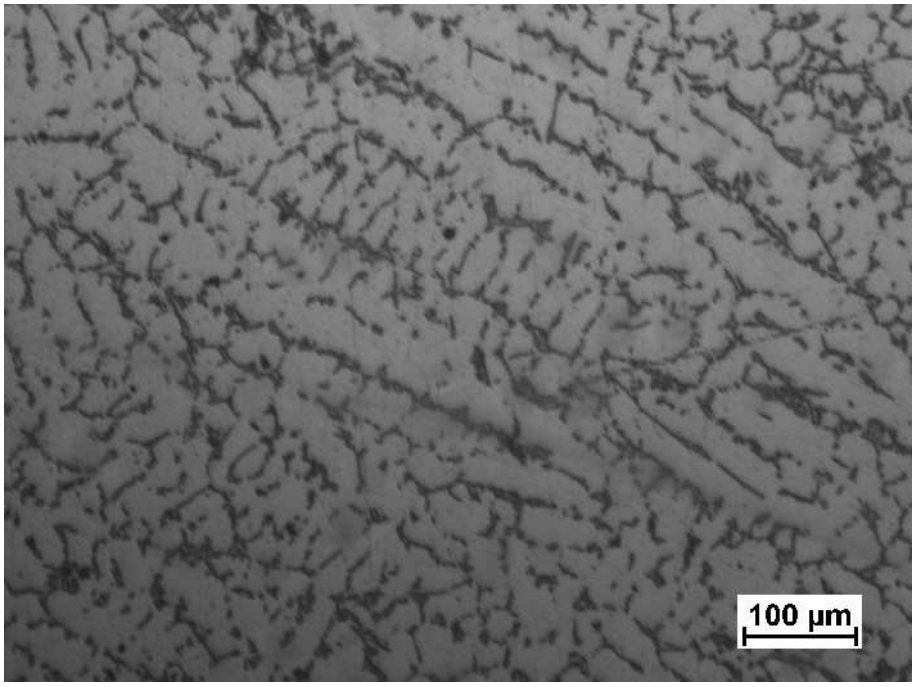

(d) 5 min UST; M= 200X

Fig. 14 continued: Microstructure comparison between samples obtained with different UST durations.

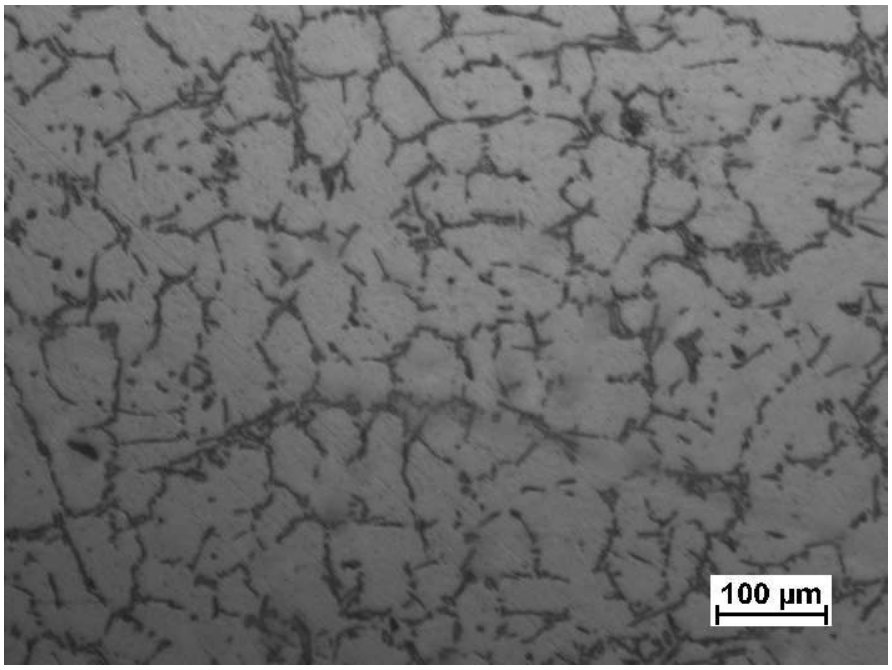

(e) 15 min UST; M= 200X

Fig. 14 continued: Microstructure comparison between samples obtained with different UST durations.

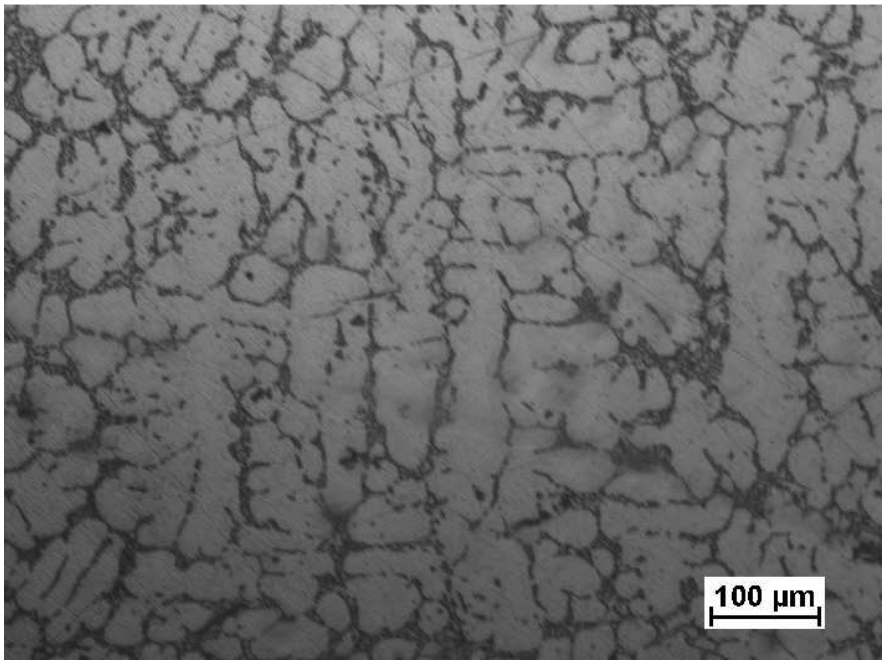

(a) T_m=400 °F (204 °C); M=200X

Fig. 15: Microstructure comparison between samples obtained with different T_m.

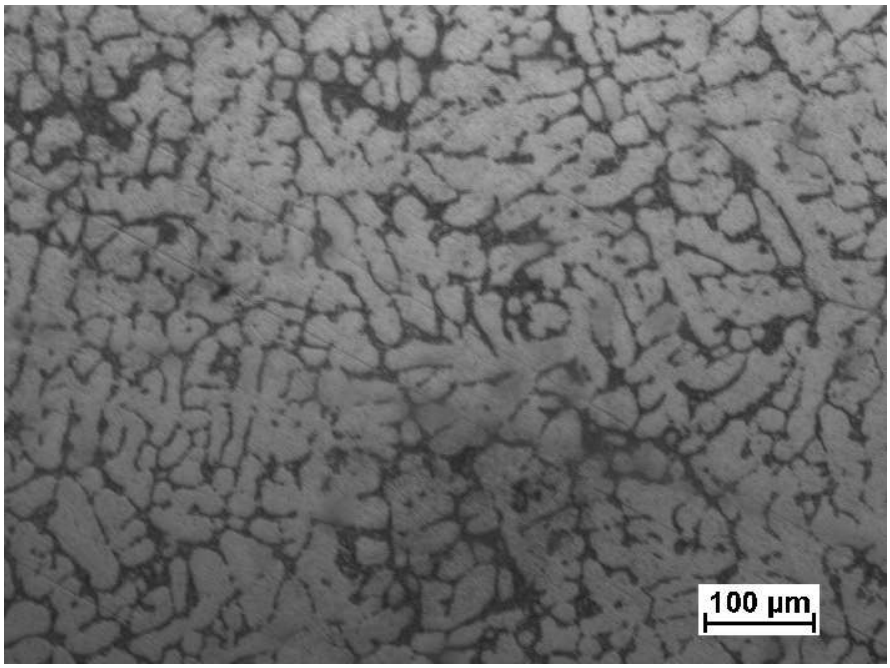

(b) T_m=600 °F (315 °C); M=200X

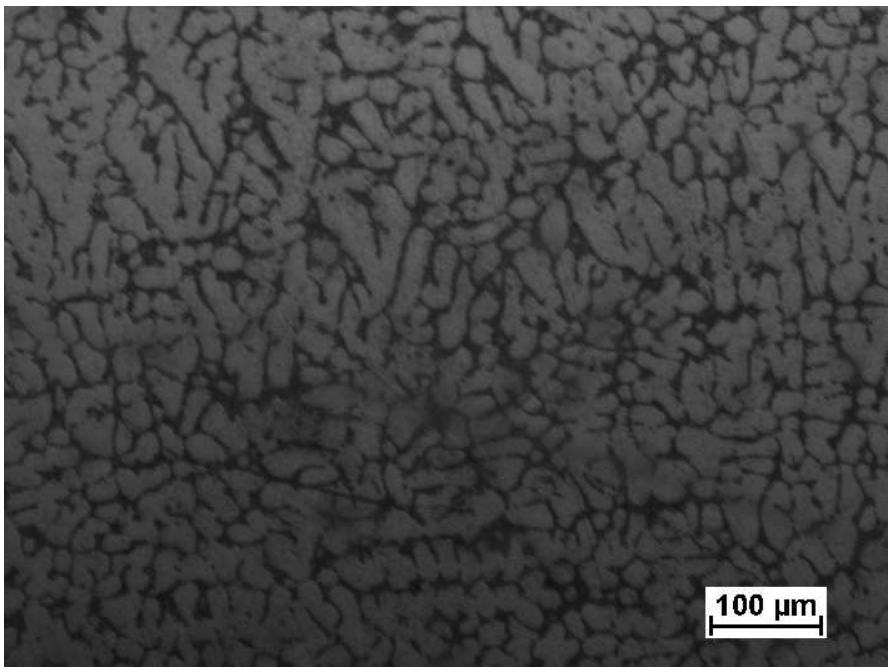

(c) T_m=800 °F (426 °C); M=200X

Fig. 15 continued: Microstructure comparison between samples obtained with different T_m.

Tables 3 present the effects of UST processing time and mold temperature on the SDAS (secondary dendrite arm spacing) based on Figs. 15. The SDAS were measured from the micrographs. According to Table 3, the sample with Tm =400 °F (204 °C) have the SDAS decreased by 10% compared with the sample with Tm =600 °F (315 °C). And sample with Tm =600 °F (315 °C) have the SDAS decreased by 21.5% compared with the sample with Tm =800 °F (426 °C).

Table 3 The effect of mold temperature on the SDAS and Eutectic Spacing (Permanent mold samples, 15 min UST)

Effect of $\mathbf{T_m}$	SDAS μm	Average μm
T_m =400 °F (204 °C)	20.6	18.1
	18.8	
	14.8	
T_m =600 °F (315 °C)	17.6	20.1
	21.2	
	21.4	
T_m =800 °F (426 °C)	31.1	25.6
	20.4	
	25.3	

4.2 DETERMINATION OF MECHANICAL PROPERTIES

Tensile test specimen dimensions are shown in Fig. 17. As shown in Table 4, after optimized T6 heat treatment, a mechanical testing was performed to evaluate tensile strength, yield strength and elongation. By using the UST treatment the tensile strength increased by at least 10% and the elongation levels by at least 20% in all studied samples when compared to the ones without the UST treatment.

Table 4 Tensile Testing Results

Permanent mold samples	Tensile strength MPa	Standard derivation MPa	Yield strength MPa	Standard derivation MPa	Elongation %	Standard derivation MPa
Without UST	227.8	4.0	180	3.2	4.0	0.30
With UST	250.2	5.2	190	3.4	4.9	0.33

Figure 16 show the cooling curves obtained by pouring the melt into a sand mold-pouring cup. In Figure 16, t_f is the estimated solidification time. It can be seen from Fig. 16 that the solidification of the UST process sample is about 5% shorter than the one processed without UST. The solidification time of the primary phase was 158s for the UST sample and 167s for the non-UST sample. The solidification time of the eutectic phase was 309s for the UST sample 328s for the non-UST sample. This is because of the UST-grain refinement and modification effects.

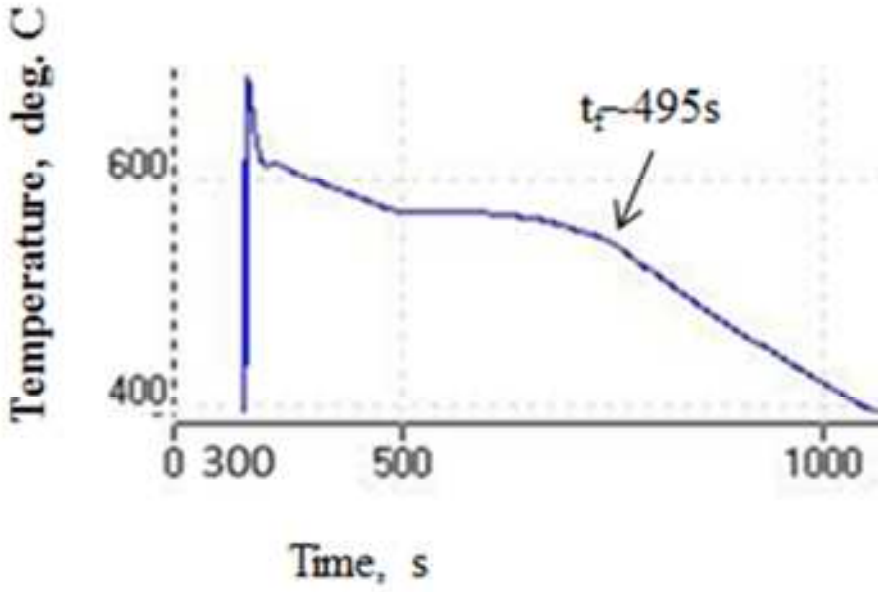

(a)

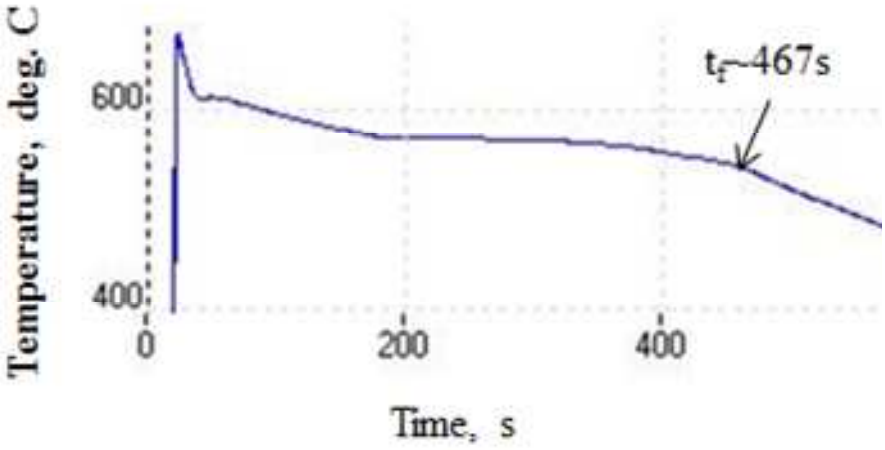

(b)

Fig. 16: Cooling curves obtained from the A356 pouring cup samples: (a) without UST and (b) with UST.

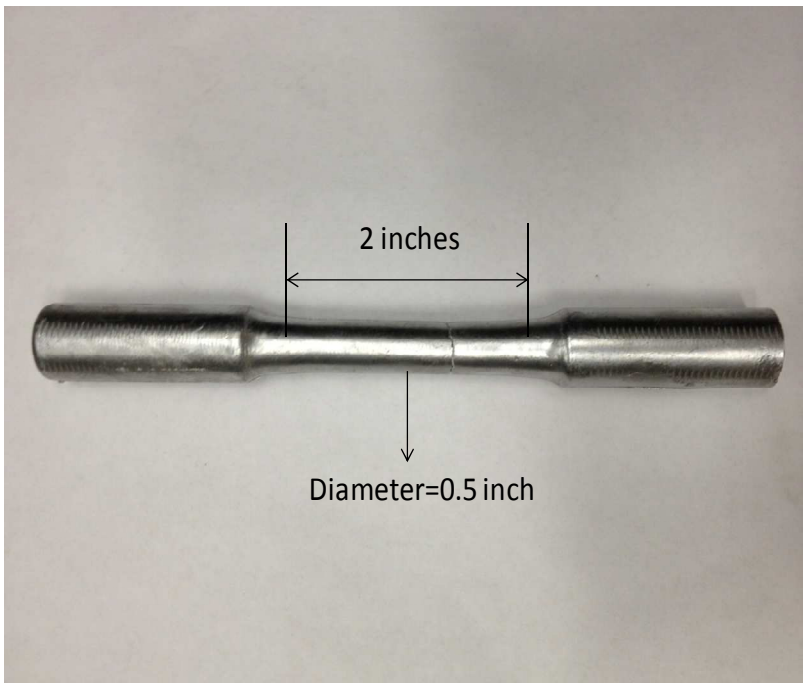

Fig. 17: Tensile test spicemen

5.0 CONCLUDING REMARKS AND FUTURE WORK

- Conclusions:

- In this study, processing equipments and parameters for casting of A356 alloy using the Ultrasonic Stirring Effects (UST) process were developed, along with characterization of the cast alloy produced at relatively high superheats which is used in foundry practice.
  - The operating conditions were determined by using a UST modeling software tool that was recently developed and validated [66, 67]. The UST modeling software tool is used for modeling and simulating the acoustic streaming and ultrasonic cavitation as well as the microstructure evolution during the solidification of cast alloys.

- The ultrasonically-stirred A356 alloy shows superior microstructure characteristics with very low microporosity levels. The samples without UST treatment have coarser microstructures than the ones with UST. It can be seen that the columnar dendritic structure was broken up because of the UST treatment. Basically, more equiaxed dendritic structure can be observed in the micrographs obtained via UST. Also, it can be seen that the Si eutectic structure (black area) is more modified. By using the UST treatment the tensile strength increased by at least 10% and the elongation levels by at least 20% in all studied samples when compared to the ones without the UST treatment.

- By using the silica sand cooling cup instead of metal mold, the grain size appeared bigger but the positive effects on microstructures of A356 alloy can still be observed. This

means the cooling rate and the UST processing both contribute to the microstructure of A356 alloy significantly. The further study by using three different mold temperatures confirmed that higher cooling rate will decrease the size of grains. It means that in order to achieve the minimum grain size, UST should be combined with high cooling rates.

- Future Work:
  - Future work will include casting experiments at low superheat (lower than 10 deg. C) in the presence of UST using a specially designed two-zone furnace by Inductotherm.
    - A parametric study will be performed to determine the effects of key ultrasonic parameters, such as power, depth of the ultrasonic probe into the melt, etc.
  - A recently developed CFD model that can simulate ultrasonic cavitation, acoustic streaming as well as microstructure evolution during the solidification of castings will be further validated and then applied to optimize future UST experiments.

REFERENCES

[1]Abramov, O.V. 1972. Kristallizaciia Metallov v Ultrazvukovom Pole. *Moscow: Metallurgiia*:256.

[2]Abramov, O.V., ed. 1994. *Ultrasound in Liquid and Solid Metals*. Vol. 493. Boca Raton: CRC Press.

[3]Abramov, V., O. Abramov, V. Bulgakov, and F. Sommer. 1998. Solidification of aluminium alloys under ultrasonic irradiation using water-cooled resonator. *Materials Letters* 37 (1–2):27-34.

[4]Abramov, V. O., O. V. Abramov, F. Sommer, and D. Orlov. 1995. Properties of Al-Pb base alloys applying electromagnetic forces and ultrasonic vibration during casting. *Materials Letters* 23 (1–3):17-20.

[5]Atamanenko TV, Eskin DG, Katgerman L. 2007. Structure Refinement by Means of (Ultrasonic) Cavitation Melt Treatment. *Aluminum Cast House Technology*.

[6]Atamanenko TV, Eskin DG, Katgerman L, ed. 2009. *Influence of ultrasonic melt treatment on structure formation in aluminium alloys with high amount of transition metals*. Edited by G. Bearne.

[7]Brennen, Christopher Earls. 1995. CAVITATION AND BUBBLE DYNAMICS: Oxford University Press.

[8]C. J. Paradies, G. T. Kim, M. E. Glicksman and R. N. Smith. 1993. The Effects of Varying Melt Flow Velocity on the Grain Fragmentation in a Mushy Zone. *TMS Light Metals Transactions*:779-782.

[9]C. Mahato, M. Shamsuzzoha and N. El-Kaddah. 2004. Solidification Morphology and Structure of Cast Al-Li 2090 Alloy at Low Superheats. *Solidification of Aluminum Alloys*:321-328.

[10]Campbell, J. 1981. Effects of Vibration during Solidification. *International Metals Reviews* 26:71-108.

[11]Campbell, John, ed. 2003. *Castings*. second edition ed: Butterworth Heinemann: London, Elsevier.

[12]Chalmers, B., ed. 1964. *Principles of Solidification*. Vol. 319. New York: John Wiley and Sons.

[13]Czerwinski, F. 2005. Near-liquidus molding of Mg–Al and Mg–Al–Zn alloys. *Acta Materialia* 53:1973-1984.

[14]Czerwinski, F. 2008. Fundamentals of Semisolid Magnesium Molding. *Journal of Metals* 60:82-86.

[15]D. M. Herlach, K. Eckler, A. Karma and M. Schwarz. 2001. Grain Refinement Through Fragmentation of Dendrites in Undercooled Melts. *Materials Science and Engineering A* 304-306:20-25.

[16]DK, Chernov. 1950. Nauka Metallakh. *Moscow: Metallurgizdat*:563.

[17]Eskin, D.G. 1996. *Z Metallkd* 87:295–299.

[18]Eskin, G. I. 1994. Influence of cavitation treatment of melts on the processes of nucleation and growth of crystals during solidification of ingots and castings from light alloys. *Ultrasonics Sonochemistry* 1 (1):S59-S6.

[19]Eskin, G.I. 1994. Ultrasonics Sonochemistry. 1 (1):S59.

[20]Eskin, G.I. 1997. Principles of Ultrasonic Treatment: Application for Light Alloys Melts. *Advanced Performance Materials* 4:223-232.

[21]Eskin, G.I. 2001. Ultrasonics Sonochemistry. 8 (3):S319.

[22]Eskin, G.I. 2002. Effect of Ultrasonic (Cavitation) Treatment of the Melt on the Microstructure Evolution during Solidification of Aluminum Alloy Ingots. *Zeitschrift fuer Metallkunde* 93:502-506.

[23]Eskin, G.I. 2005. Nedendritnaia Kristallizaciia Legkich Splavov: Itogi I Perspektivy. *Liteinoe Proizvodstvo* 1-4:94-104.

[24]Eskin, G.I., ed. 1998. *Ultrasonic Treatment of Light Alloy Melts*. Amsterdam: Gordon & Breach.

[25]Eustathopoulos N, Drevet B. 1998. Determination of the nature of metal-oxide interfacial interactions from sessile drop data. *Mater. Sci. Eng. A* 249:176-180.

[26]Flemings, ed. 1974. *Solidification Processing*: McGraw Hill Inc.

[27]Flood, S.C., Hunt, J.D. 1981. Modification of Al–Si Eutectic Alloys with Na. *Metal science* 15:287–294.

[28]G. I. Eskin. 2001. Broad prospects for commercial application of the ultrasonic (cavitation) melt treatment of light alloys,. *Ultrasonics Sonochemistry* 8 (3):319–325.

[29]G.I. Eskin, D.G. Eskin. 2002. Effects of ultrasonic (cavitation) melt processing on the structure refinement and property improvement of cast and worked aluminium alloys. *Materials Science Forum* 396-402:77-82.

[30]Gabathuler JP, Barras D. 1992. Evaluation of Various Process of The Production of Billets with Thixotropic Conference properties. *2nd int. conf. on semisolid alloys and comp., MIT/Boston,*:33-46.

[31]Greer, A. L. 1991. Grain refinement in rapidly solidified alloys. *Materials Science and Engineering: A* 133:16-21.

[32]Greer, AL. 2003. *Phil Trans Math Phys Eng Sci* 361:479-495.

[33]H. Yasuda, N. Nakatsuka, T. Nagira, A. Sugiyama, M.Yoshiya,, and K.Umetani K.Uesugi. 2009. X-ray imaging study on grain refinement due to dendrite fragmentation. *Proc. 6th Electromagnetic Processing of Materials*:257-260.

[34]Haghayeghi, R., and L. Nastac. 2011. On microstructural refinement of an AA7449 aluminium alloy through shearing above liquidus temperature. *Materials Letters* 65 (21–22):3230-3233.

[35]Han, Y., Li, K., Wang, J., Shu, D. and Sun, B. 2005. Influence of high-intensity ultrasound on grain refining performance of Al-5Ti-1B master alloy on aluminium. *Materials Science and Engineering A* 405:306-312.

[36]Hanbing Xu, Xiaogang Jian, Thomas T. Meek, and Qingyou Han. 2004. Degassing of Molten Aluminum A356 Alloy Using Ultrasonic Vibration. *Materials Letters* 58 (29):3669–3673

[37]Hem, S.L. 1967. The Effect of Ultrasonic Vibrations on Crystallization Processes. *Ultrasonics* 5:202-207.

[38]I. G. Brodova, P. S. Popel and G. I. Eskin. 2002. Liquid metal processing: applications to aluminum alloy production.

[39]J. Campbell, 2 (1981) 71. 1981. Effects of vibration during solidification. *International Metals Reviews* 2:71.

[40]J. F. Li, Y. C. Liu, Y. L. Lu, G. C. Yang and Y. H. Zhou. 1998. Structural evolution of undercooled Ni-Cu alloys. *Journal of Crystal Growth* 192:462-470.

[41]Jian, X., Meek, T.T., Han, Q. 2006. Refinement of Eutectic Silicon Phase of Aluminum A356 Alloy Using High-Intensity Ultrasonic Vibration. *Scripta Materialia* 54:893–896.

[42]Jian, X., H. Xu, T. T. Meek, and Q. Han. 2005. Effect of power ultrasound on solidification of aluminum A356 alloy. *Materials Letters* 59 (2–3):190-193.

[43]Khalifa, W., Y. Tsunekawa, and M. Okumiya. 2008. Effect of ultrasonic melt treatment on microstructure of A356 aluminium cast alloys. *International Journal of Cast Metals Research* 21 (1-4):129-134.

[44]Lee, J., Kentish, S., Matula, T.J. and Ashokkumar, M. 2005. Effect of surfactants on inertial cavitation activity in a pulsed acoustic field. *Journal of Physical Chemistry B* 109:16860-16865.

[45]Ludtka, G. M., Jaramillo, R. A., Kisner, R. A., Mackiewicz-Ludtka, G. and Wilgen, J. B. April 2005. Exploring Ultrahigh Magnetic Field Processing of Materials for Developing Customized Microstructures and Enhanced Performance. Oak Ridge National Laboratory Technical Report.

[46]M. Li, G. Yang and Y. Zhou. 1999. Direct observation of fragments of primary dendrite from undercooled Fe-Co alloys. *Journal of Crystal Growth* 204:413-417.

[47]M. Schwarz, A. Karma, K. Eckler and D. M. Herlach, and 1380. 1994. Physical Mechanism of Grain Refinement in Solidification of Undercooled Melts. *Physical Review Letters* 73:1380.

[48]Meek, T.T., Han, Q., Ultrasonic Processing of Materials., U.S. Department of Energy, USA, (accessed 9.01.10.) (2006). Ultrasonic Processing of Materials.

[49]Murty BS, Kori SA, Chakraborty M. 2002. Grain refinement of Al and its alloys by heterogeneous nucleation and alloying. *Int Mater Rev* 47:2-29.

[50]Nastac, L. Numerical Modeling of Solidification Morphologies and Segregation Patterns in Cast Dendritic Alloys. *Acta Materialia* 47 (17):4253-4262.

[51]Nastac, L. 2011. Mathematical Modeling of the Solidification Microstructure Evolution in the Presence of Ultrasonic Stirring. *Metallurgical and Materials Transactions B* 24:1297-1305.

[52]Nastac, L. 2012. Multiscale Modeling of the Solidification Microstructure Evolution in the Presence of Ultrasonic Stirring. *IOP Conference Series: Materials Science and Engineering* 33:012079.

[53]Nastac, L., ed. 2004. *Modeling and Simulation of Microstructure Evolution in Solidifying Alloys*: Springer.

[54]Neppiras, E.A. and Noltingk, B.E. 1951. Cavitation produced by ultrasonics: theoretical conditions for the onset of cavitation. *Proc. Phys. Soc., London* 64B:1032--1038.

[55]Noltingk, B.E. and Neppiras, E.A. 1950. Cavitation produced by ultrasonics. *Proc. Phys. Soc., London* 63B,: 674--685.

[56]P. K. Galenko, G. Phanikumar, O. Funke, L. Chernova, S. Reutzel, M. Kolbe and D. M., and Herlach. 2007. Dendritic solidification and fragmentation in undercooled Ni-Zr alloys. *Materials Science and Engineering: A* 449-451:649-653.

[57]Prosperetti, A. . 1984. Bubble phenomena in sound fields: part one and part two. *Ultrasonics* 22:69--77 and 115--124.

[58]Rappaz, J. A. Dantzig and M., ed. 2009. *Solidification*. Boca Raton: CRC Press.

[59]Rappaz, S. Vernede and M. 2007. A simple and efficient model for mesoscale solidification simulation of globular grain structures. *Acta Materialia* 55:1703-1710.

[60]Rozenberg, L.D., ed. 1969. *Sources of High-Intensity Ultrasound*. Vol. 1-2. New York: Plenum Press.

[61]Ruvalcaba, D., Mathiesen, R.H., Eskin, D.G., Arnberg, L., Katgerman, L. 2007. In Situ Observation of Dendritic Fragmentation Due to Local Solute-Enrichment during Directional Solidification of an Aluminum Alloy. *Acta Materialia* 55:4287–4292.

[62]Southin, R.T. 1966. The Influence of Low-Frequency Vibration on the Nucleation of Solidifying Metals. *Journal of the Institute of Metals* 94:401-407.

[63]Stefanescu, Doru Michael. 2008. *Science and Engineering of Casting Solidification*: New York : Springer Oct. 2008 2nd ed.

[64]T. Campanella, C. Charbon and M. Rappaz. 2003. Influence of permeability on the grain refinement induced by forced convection in copper-base alloys. *Scripta Materialia* 49:1029-1034.

[65]T. T. Meek, X. Jian, H. Xu and Q. HanReport ORNL/TM-2005/125, US Department of, and Washington DC Energy, USA, 2006. 2006. Ultrasonic processing of materials. Washington DC, USA: US Department of Energy.

[66]Vives, C. 1992. *2nd int. conf. on semisolid alloys and comp., MIT/Boston,*:436-439.

[67]Warner TJ, Shahani RA, Lassince P, Raynaud GM. 1997. Aluminum alloy developments for affordable airframe structures. *ASM International conference, Paris, France*:12.

[68]Y. Z. Chen, F. Liu, G. C. Yang, N. Liu, C. L. Yang, H. Xie and Y. H. Zhou. 2008. Grain refinement of Fe75Ni25 alloys at low undercooling. *Materials Characterization* 59:412-416.

[69]Yasuda, H., Yamamoto, Y., Nakatsuka, N., Nagira, T., Yoshiya, M., Sugiyama, A., Ohnaka, I., Umetani, K., Uesugi, K. 2008. In Situ Observation of Nucleation, Fragmentation and Microstructure Evolution In Sn–Bi And Al–Cu Alloys. *International Journal of Cast Metals Research* 21 (1):125-128.

[70]Z. Fan , Y. Wang, M. Xia, S. Arumuganathar. 2009. Enhanced heterogeneous nucleation in AZ91D alloy by intensive melt shearing. *Acta Materialia* 57:4891–901.